ENHANCED COMPRESSOR DISTORTION TOLERANCE USING ASYMMETRIC INLET GUIDE VANE STAGGER

by

Andreas Schulmeyer

B.S., University of Illinois, (1987)

SUMMITED IN PARTIAL FULFILLMENT

OF THE REQUIREMENTS FOR THE DEGREE OF

MASTER OF SCIENCE

IN AERONAUTICS AND ASTRONAUTICS

at the

MASSACHUSETTS INSTITUTE OF TECHNOLOGY

August 1989

Signiture of Author_____
Department of Aeronautics and Astronautics, August, 1989

Certified by_____
Professor Edward M. Greitzer
Thesis Supervisor
Department of Aeronautics and Astronautics

Accepted by_____
Professor Harold Y. Wachman
Chairman, Department Graduate Committee

Enhanced Compressor Distortion Tolerance Using Asymmetric Inlet Guide Vane Stagger

by
Andreas Schulmeyer

Submitted to the Department of Aeronautics and Astronautics
on August 28, 1989 in partial fulfillment of the
requirements for the Degree of Master of Science
in Aeronautics and Astronautics

ABSTRACT

This work is experimental verification of a method to increase axial compressor distortion tollerance. The method uses a restagger of the inlet guide vanes to achieve the desired uniform inlet velocity profile. In order to achieve this the vanes are opened in the low total pressure region, increasing mass flow and pressure rise in this section, and closing the vanes in the high total pressure region to reduce the mass flow and pressure rise in this section of the compressor.

The theoretical calculations showed that a ten degree restagger of the guide vanes would achieve the desired result for a one dynamic head total pressure distortion. This setup was then tested on the MIT low-speed single stage compressor. The test data showed the improved performance of the restaggered compressor. The non-uniformity in the inlet velocity is reduced by 50%, while presssure rise at stall is 5.3% higher than without the restagger and the stall flow coefficient is 2.7% higher.

Thesis Supervisor: Edward M. Greitzer

Title: Professor of Aeronautics and Astronautics

ACKNOWLEDGEMENTS

I would like to offer my thanks to my advisor, Professor E.M. Greitzer, for his support in solving many of the unexpected mysteries that the experimental results provided.

Thanks to Gwo-Tung Chen for his theoretical work which set the basis for this experimental investigation as well as the patient introduction he gave me to the methods of this scheme.

I also appreciate all the help provided by Viktor Dubrowski, Roy Andrew, Jim Nash and Jerry Guenette with the experimental setup.

I would also like to thank all my friends at the GTL and at Ashdown for making life at MIT so much more enjoyable.

Most of all I would like to thank my parents, Gerhard and Helga Schulmeyer, for all their love and encouragement that have made it possible for me to be where I am.

This work was supported by the Air Force Office of Scientific Research under contract AFOSR -87- 0398E.

TABLE OF CONTENTS

LIST OF TABLES

LIST OF FIGURES

List of Symbols

C	Velocity
Ci	Blade chord
cp	Pressure rise coefficient across blade row
P	Non-dimensional pressure
R	Mean radius
r	Blade stagger angle
α	Absolute flow angle
γ	Blade stagger angle
ϕ	Flow coefficient
ρ	Density
θ	Circumferential angle
Ψ	Compressor pressure rise

Subscipts

e	Exit
in	Inlet
t	Total
x	Axial
y	Circumferential

Chapter 1 Introduction

Inlet distortion tolerance is an important factor affecting the stall margin in modern axial compressors. Up to one half of the design stall margin (Figure 1.1) may be allocated to account for the effect of inlet distortion [1]. This margin allows for the non-uniformities in the inlet flow due to such phenomena as crosswind, high angle of attack induced inlet seperation or shock-boundary layer interaction in supersonic inlets. In addition to decreases in pressure rise and efficiency of the compressor, possible effects of inlet distortion are rotating stall, combustion flame out or engine overheating.

For these reasons the effect of inlet distortion on axial compressors has received much attention in the past years. Methods have been developed to predict performance [2,3,4] and stability [5,6] of a compressor operating with an inlet distortion. The standard methods to reduce engine succeptability to distortion are to increase the tolerance to non-uniformities by modifying the engine inlets, or to lower the operating point to increase the stall margin.

With the capabilities of new electronic controls other methods to increase distortion tolerance have become available. The theoretical capability to control the stagger setting of each individual inlet guide vane (IGV) or stator blade [7] allows the compressor to be divided into two or more 'parallel compressors', with an asymmetric restaggering patern chosen to match the inlet distortion [8]. By opening

the vanes in the low total pressure region the flow coefficient is increased and the operating point moves away from stall. In the high total pressure region the vanes are closed and the flow coefficient is reduced, however, because this region is operating far from stall the reduction in flow coefficient does not pose a problem.

The behaviour of a compressor restaggered in this manner can be shown qualitatively in the response of a parallel compressor to a inlet total pressure distortion. The low total pressure zone and the high total pressure zone operating points are determined by the magnitude of the inlet distortion and the slope of the compressor characteristic (Figure 1.2). This leads to a different flow coefficient in the two regions, with the low pressure zone operating closer to stall. A non-axisymmetric vane stagger reduces this velocity non-uniformity by shifting the low total pressure region speedline to the right and the high total pressure region speedline to the left (Figure 1.3). The result of the restaggering is a more uniform flow coefficient around the compressor circumference and an increase in stall margin gained by moving the low total pressure operating point further from stall.

A further benefit of using this method is that the mass averaged pressure rise is not reduced as much as when closing all vanes uniformly. A second benefit in terms of overall engine performance is that the compressor can deliver a uniform flow to the combustor thus reducing the

likelyhood of developing hot spots that can damage the turbine.

The object of this thesis is to experimentally demonstrate this type of scheme for improving inlet distortion tolerance of an existing compressor. The test vehicle is the single stage compressor at the MIT Gas Turbine Laboratory. The results of the experiment are described in this thesis.

Chapter 2 Theoretical Model and Calculations

2.1) Introduction

The theoretical calculations performed as part of the distortion control are the application to a specific single stage compressor of the method described by Chen et al. for axial compressors. The work in [8] consisted of calculating the characteristics for a three stage compressor and implementing the control sceme on this compressor. The procedure used to calculate the off-design performance was shown to lead to speedlines in agreement with experimental data. The computations also indicated that the distortion control is capable of reducing the velocity defect due to a distortion of greater than two dynamic heads by a factor of two (Figure 2.1).

This chapter deals with the prediction of the compressor characteristic, a summary of the distortion computations and the application of the computations to the single stage compressor.

2.2) Compressor Characteristic Calculation

The program used to calculate the off-design behaviour of the compressor was written by Chen [8] based on a model proposed by Raw and Weir [9]. Losses are calculated for the blade rows by using a loss parameter based on the diffusion factor (Figure 2.2), with a multiplication factor dependent

on blade Reynolds number (Figure 2.3) applied. Carter's rule for deviation is modified by an 'adder' which is a function of the diffusion factor of the blade rows (Figure 2.4).

The major assumptions of the analysis are:

- high hub to tip ratio, so mean line velocity triangles are used
- low Mach number so compressibility is neglected
- blades are represented by circular arcs

The last assumption leads to deviations in reasonable agreement with experimental data, as the turning is overestimated by neglecting real fluid effect and by neglecting thickness turning is underestimated. These two effects are of comparable magnitude [10] for a solidity of order one, the solidity of the rotor and stator rows in the experimental compressor.

The required inputs to the program are the rotor and stator camber and stagger angles and the IGV leaving angle. The compressor characteristic and the flow angles are then calculated for any desired range of flow coefficients.

For the three stage compressors used in previous calculations the agreement between the calculated and experimentally obtained speedlines is close enough for the control calculations that followed (Figure 2.5).

The results for the single stage compressor, however, showed a characteristic that continues to rise as the flow coefficient deceases (Figure 2.6). From these calculations it was not possible to predict the compressor stall point (or the pressure rise at stall) with any precision. The

model does not perform satisfactorally for the single stage compressor possibly because the correlations used to predict losses are optimized for multi-stage compressors. The factors are thus optimized for multi-stage compressors.

Even though the program calculated speedlines that are not comparable to the experimental speedlines, that were later obtained (Figure 2.7), the calculated curves were used to determine the amount and location of restaggering required to reduce the magnitude of the velocity distortion. The restaggering calculations are possible with the calculated speedlines as the method uses the relative changes in pressure rise due to a change in stagger and the slope of the characteristic as the relevant parameters. For the actual amount of restaggering required the experimental speedlines could then be used to repeat the calculations. To find the optimum restaggering method the calculated speedlines were then used with the point of inflection, the point where the calculated speedline is the 'flattest', as the calculated 'stall' point.

The program was then used to calculate various speedlines. The final compressor geometry can be found in table 2.1 and the calculated characteristic in figure 2.6. The stacking of the speedlines required for this control scheme is shown in figure 2.8 where the nominal speedline is bracketed by the speedlines with a 10 degree opening and closing of the IGVs and stators. From this family of curves the parameters necessary for the restaggering calculations,

$\partial\Psi/\partial\phi$ and $\partial\Psi/\partial\gamma$, can be obtained.

2.3) Distortion Theory Summary

This section is a summary of the theory developed by Chen for a compressor operating with a steady inlet distortion. The pressure rise across a blade row is given by an axisymmetric part and an asymmetric component due to the fluid acceleration within the blade row. The fluid mechanics for compressor response to total pressure inlet distortion is described in [5].

With a linearized upstream and downstream flowfield the compressor performance is given by

$$\tilde{P}_e - \tilde{P}_{tin} = \Psi(\phi,\gamma) - \lambda\frac{\partial\phi}{\partial\theta} \qquad (2.1)$$

where

$$\lambda = \sum_{i=1}^{N}\frac{C_i}{\cos\tau_i R_i}$$

is the parameter associated with fluid acceleration within the blade rows. C, r, R are the chord, stagger and mean radius, respectively, of the rotor.

For a small disturbance the downstream pressure field satisfies

$$\nabla^2 P_e = 0 \qquad (2.2)$$

and the boundary condition at the compressor exit plane is

$$-\frac{1}{\rho}\frac{\partial P_e}{\partial x}\bigg|_{x=0} = C_x\frac{\partial C_x}{\partial x} + C_y\frac{\partial C_x}{\partial y}\bigg|_{x=0} \qquad (2.3)$$

The linearized results obtained from perturbing Eq.(2.2) and (2.3) are

$$\delta\tilde{P}_e - \delta\tilde{P}_{tin} = \frac{\partial\Psi}{\partial\phi}\delta\phi + \frac{\partial\Psi}{\partial\gamma}\delta\gamma - \lambda\frac{\partial\delta\phi}{\partial\theta} \tag{2.4}$$

and

$$\left.\frac{\partial\delta\tilde{P}_e}{\partial\tilde{x}}\right|_{x=0} = \phi^2\sec^2\alpha\left.\frac{\partial\delta\alpha}{\partial\theta}\right|_{x=0} \tag{2.5}$$

Expanding all variables in Fourier series

$$\delta\tilde{P}_e = \sum_{n=-\infty}^{+\infty} a_n e^{in\theta}e^{-i|n|x} \tag{2.6}$$

$$\delta\tilde{P}_{tin} = \sum_{n=-\infty}^{+\infty} e_n e^{in\theta} \tag{2.7}$$

$$\delta\phi = \sum_{n=-\infty}^{+\infty} b_n e^{in\theta} \tag{2.8}$$

$$\delta\gamma = \sum_{n=-\infty}^{+\infty} d_n e^{in\theta} \tag{2.9}$$

and subsituting Eq. (2.6),(2.8) and (2.9) into Eq. (2.5) we have

$$a_n = \frac{in}{|n|}\phi^2\sec^2\alpha\left(\frac{\partial\alpha}{\partial\phi}b_n + \frac{\partial\alpha}{\partial\gamma}d_n\right) \tag{2.10}$$

Combining (2.4),(2.7),(2.8),(2.9) and (2.10)

$$b_n = -\frac{\left(\frac{\partial\Psi}{\partial\gamma} + \frac{in}{|n|}\phi^2\sec^2\alpha\frac{\partial\alpha}{\partial\gamma}\right)d_n + e_n}{\frac{\partial\Psi}{\partial\gamma} - in\lambda + \phi^2\sec^2\alpha\frac{in}{|n|}\frac{\partial\alpha}{\partial\phi}} \tag{2.11}$$

The stagger distribution that eliminates the velocity distortion, i.e.

$$\delta\phi = 0\,, \qquad b_n = 0 \tag{2.12}$$

is given by

$$\frac{d_n}{e_n} = \frac{-1}{\frac{\partial\Psi}{\partial\gamma} + \frac{in}{|n|}\phi^2 \sec^2\alpha \frac{\partial\alpha}{\partial\gamma}} \tag{2.13}$$

2.4) Restaggering Scheme Calculations

The program that calculates the characteristics for the compressor also provides the two variables $\partial\Psi/\partial\gamma$ and $\partial\Psi/\partial\phi$ that determine the behaviour of the compressor with an inlet distortion and the implemented restagger. These two derivatives are needed to to calculate the velocity profile of the compressor with an inlet total pressure distortion and various stagger profiles. The goal is to find a stagger profile to minimize the velocity non-uniformity at the face of the compressor. For the calculations the inlet total pressure distortion is a sine shaped defect over 180 degrees of the annulus with a magnitude of one dynamic head (Figure 2.9).

Based on the work done by Chen two schemes were used in the first set of calculations. The first is a restagger of both IGVs and stators identical amounts in phase with the total pressure distortion. The results can be seen in the resulting axial velocity distribution for the compressor operating near stall (Figure 2.10) and at design flow

(Figure 2.11). For both of these the velocity defect due to the distortion are of the same shape and magnitude, as in both cases the slope of the characteristic and $\partial\Psi/\partial\gamma$ are almost identical. The capability to correct the velocity defect at both flow coefficients is also of the same order resulting in almost identical behavior for both cases. The magnitude of the velocity distortion is reduced by almost a factor of two for both flows although there is still a defect remaining. It is not possible to reduce the velocity non-uniformity any further with this scheme, as a larger restaggering leads to an overcorrection in parts of the circumference, which can be seen in the 15 degree restagger of the blade rows.

This led to the attempt to reduce the velocity distortion by restaggering the stators and IGVs differing amounts, still in phase with the pressure distortion. A sampling of the resultant velocity profiles, of the case where the stator restagger is 3/4th of the IGV restagger, can be seen in figures 2.12 and 2.13. Here again it was possible to reduce the velocity distortion by a factor of two, but the velocity profile still shows the same behaviour as the previous calculations.

The next step allowed for a phase shift between the restaggered regions and the pressure distortion. The model was extended in this case to allow for the phase shift between the restaggering in the two blade rows. In this case the repsonse to a stator restagger is calculated separately

from the response to a IGV restagger. This extension of the model assumes that the velocity perturbations introduced by the restagger of the stators does not alter the velocity perturbation introduced by the IGVs if both are calculated separately and vice versa. This is possible as the linearization in the model assumes that $\partial\Psi/\partial\gamma$ and $\partial\Psi/\partial\phi$ remain constant even with the velocity perturbations introduced by the total pressure distortion, or in this case by the restagger of the other blade row. The final result is then obtained by summing the effect of the individual blade row restaggerings. This method introduces the phase shift as a new degree of freedom and should thus lead to an improved velocity profile.

As figures 2.14 and 2.15 show a reduction of the flow non-uniformity can be achived in this manner. The magnitude of the velocity distortion can be reduced by a factor of four or more. The complexity of this scheme, however, detracts from its attractiveness so that further schemes were tested.

The most efficient method to reduce the velocity distortion was found to require a restaggering of the IGVs only. This method (Figures 2.16 and 2.17) is capable of completly removing the velocity distortion, but it is limited by the amount of restagger of the IGVs possible without separating the airfoils.

It was decided to use only the restaggering of the IGVs as the scheme to be implemented. The magnitude of restaggering is then dependent on the size of the pressure

distortion, the change in pressure rise due to the change in stagger, $\partial\Psi/\partial\gamma$, and the maximum restaggering possible without stalling the blades.

Chapter 3 Experimental Setup

3.1) Introduction

The GTL single stage compressor was modified for the experimental investigation. The major changes were the restaggering of the blade rows, the reduction of stage spacing, the installation of a distortion screen and added instrumentation and modification of the data aquisition programs. The compressor has a hub to tip ratio of 0.74 and the design flow rate for the baseline blade setting is 0.59. A detailed description of the geometry is given in table 2.1.

3.2) Blading Modifications

The IGVs used previously were long chord sheet metal of high solidity. These were not suitable for the restaggering required by the distortion experiment, as the long chord led to interference with the outer casing. They also have low incidence tolerance. The replacement set of IGVs had a shorter chord thus allowing for the required movement, and, although they are also sheet metal, somewhat better incidence tolerance as they are thicker, with a rounded leading edge.

The new blades were 1/16th inch shorter than the previous set leading to a clearance around the centerbody of the compressor. As the centerbody was now supported only at the front end by six struts three of the 46 IGVs were

replaced by bolts to locate the the centerbody and eliminate vibration.

3.3) Blade Row Spacing

The compressor had been set up with maximum spacing, a 5" gap between the rotor and stator, for the previous experiment. The effect of spacing was thus investigated using an actuator disc analysis (see appendix for derivation), with rotor and stator lumped into one disc and IGVs as another. The spacing (H), non-dimensionalized by the compressor radius (R), between the two was varied from the existing setup down to zero. As the calculations show (Figure 3.1) the velocity correction introduced with minimal spacing (H/R = 0.05) is in phase with the IGV stagger movement from -90 to +90 degrees. For a larger spacing the velocity correction shifts in the direction of the turning introduced by the IGVs. This, together with the change in magnitude, will lead to an incorrect estimate in the restaggering calculations based on zero spacing. The spacing between the IGV row and the rotor was therefore reduced to the minimum possible with the existing compressor corresponding to H/R = 0.25, although this still left a significant gap.

The program that calculates the compressor response to the inlet distortion was not modified to account for this spacing between the blade rows due to time constraints on the program.

3.4) Distortion Screen Design and Placement

The screen was designed to give a total pressure distortion of one dynamic head. It consists of 7 sections which lead to an approximation of the sine shaped defect used in the calculations. The total pressure loss coefficients for each section were determined by rescaling the screen used by Bruce [11] to obtain a sinusoidal velocity profile. The circumferrential extension and the pressure loss coefficient of each section can be found in table 3.1.

The screen was attached to the forward struts supporting the centerbody 23 inches ahead of the IGVs, where it could easily be removed to obtain uniform flow compressor data. With this large spacing some mixing was expected, the total pressure profile measured at the IGV plane is shown in figure 3.2. The overall profile approximates the desired sinusoidal total pressure defect, except for the reading at -90 degrees,the interface of the low and high total pressure regions, which is lower than expected.

3.5) Instrumentation Layout

The instrumentation was set up to give a detailed circumferential profile in front of the IGV plane and to measure overall compressor performance. Twenty kiel probes, for total pressure measurement, and twenty static pressure taps were installed upstream of the IGVs. Ten more sets were installed downstream of the stator (Figure 3.3). The close

spacing of the kiel probes behind the static pressure taps led to an increase in the static pressure measured and a correction factor was calculated by representing the kiel probe and its wake as a source. The resulting correction factor of 1.08 for the axial velocity agrees with the ratio of the axial velocity measured by a pitot tube compared to that obtained from the kiel probes and static pressure taps (Figure 3.4).

Four of the static pressure taps, two at the inlet plane and two in the downstream set, were not used in the calculations as they gave incorrect readings whose origion could not be found.

The calibration curves for the two scannvalves used to obtain the pressure readings are shown in figures 3.5 and 3.6.

3.6) Experimental Procedure and Data Aquisition

The basic plan of the experiment was as follows. The compressor characteristics for IGV settings of +15, 0, -15 relative to the design staggering were first obtained. With this data $\partial\Psi/\partial\gamma$ can be calculated. This determines the amount of restaggering required to remove the velocity distortion introduced by the screen. The final speedlines would then show the difference between the uniformly and non-axisymmetricly staggered compressor and show the improvement in the circumferrential velocity profile.

The individual speedlines are taken starting with the

throttle completely open. The throttle is slowly closed to a new operating point and the procedure repeated until the stall point is reached. Each of the compressor operating points is calculated using an average of the inlet total and exit static pressures to give the total to static pressure rise. The axial velocity is calculated by averaging the local velocities obtained from the total and static pressure probes. This definition of the axial flow coefficient is also used for the distorted flow where it represents an average flow coefficient for the whole compressor.

In distorted flow the overall flow coefficient for the compressor obtained from averaging the individual velocities gave a value up to 5% higher than a method using the average pressure readings (Figure 3.7). As defined here, therefore, all axial flow coefficients are those based on the velocities at the inlet plane.

Chapter 4 Experimental Results

4.1) Compressor characteristics

The first sets of data taken were the family of speedlines needed to calculate the variables $\partial\Psi/\partial\gamma$ and $\partial\Psi/\partial\phi$. Several IGV stagger settings were used. The inital setup was an IGV stagger angle of 7.5 degrees (Figure 4.1). As expected from previous results the agreement with the calculated speedline was only acceptable near the design flow coefficient of ϕ = 0.59, so new calculations of the optimum stagger were performed using the experimentally obtained speedlines.

Two speedlines were then taken for a change of stagger of +/- 15 degrees from nominal (Figures 4.1). The increased stagger of 22.5 degrees led to a decrease in pressure rise and stall flow coefficient, as predicted by theory. The speedline with the IGV stagger setting of -7.5 degrees showed an unacceptable drop in pressure rise near stall, dropping below the pressure rise for the +7.5 degree stagger. The reason for the lower pressure rise is the separation of the airflow on the IGVs at a high negative angle of attack. As the linear model uses only a mean value of $\partial\Psi/\partial\gamma$ a change in sign of $\partial\Psi/\partial\gamma$ was inappropriate for the range of stagger angles to be used in the control sceme.

Figure 4.2 shows a speedline for a IGV stagger of 0 degrees . Using linear interpolation of the three speedlines with stagger angles of +7.5, 0 and -7.5 degrees stagger the

critical stagger for which $\partial\Psi/\partial\gamma = 0$ is at 3 degrees, which was taken as the point where the IGVs separated.

To avoid stagger angles for which the sign of $\partial\Psi/\partial\gamma$ changes a speedline was taken with an IGV stagger of 27.5 degrees (Figure 4.2). This speedline along with the speedlines for +7.5, 15 and 22.5 degress showed the desired stacking and they were chosen for the experiment (Figure 4.3).

The nominal setting around which the non-axisymmetric staggering was then designed was a stagger angle of 15 degrees which allowed for a maximum restagger of up to 10 degrees before separation occured.

The static pressure readings for undistorted flow (Figure 4.4) showed non-uniformiteis that could not be accounted for. A correction factor for each probe was therefore obtained from the raw data. The corrected velocity profile was then satisfactory near stall (Figure 4.5). The upstream struts supporting the centerbody, the eccentricity of the centerbody, the variation of the blabe tip clearence and other imperfections in the compressor are accounted for in this correction. The correction in the static pressure readings accounts for the permanent, i.e. systematic, non-uniformities in the compressor and the subsequent will show only changes due to the inlet distortion and the IGV restagger.

The same correction, to account for blade to blade variations and other imperfections of the compressor, was performed on the exit static pressure non-uniformities, but

even then it was not possible to reduce the static pressure non-uniformity at the exit plane to less than .05 dynamic heads (Figure 4.6).

4.2) Restaggering Scheme Calculations

The parameters $\partial\Psi/\partial\gamma$ and $\partial\Psi/\partial\phi$ were determined from the experimental speedlines. All speedlines were fit with a third order polynomial (Figure 4.7) and the resulting curve fits used for a calculation of $\partial\Psi/\partial\gamma$ and $\partial\Psi/\partial\phi$ at any operating point of the nominal speedline. These values (Figure 4.8 and 4.9) are compared with those calculated using the computer generated speedlines. The experimental values of $\partial\Psi/\partial\gamma$ and $\partial\Psi/\partial\phi$ were used to find the restaggering required to reduce the velocity non-uniformity created by the distortion screen. For the 1.0 dynamic head total pressure distortion a restagger of 10 degrees was needed (Figures 4.10 and 4.11) to obtain a sizable reduction in the velocity distortion.

The actual restagger of the IGVs was a square wave with a +10 degree restagger in the low pressure zone and a -10 degree restagger in the high pressure region. The square wave restagger was chosen as a simple sector restaggering that would show a benefit similar to the more complicated method of a sinusoidal restagger, where each blade would have to be restaggered by a different amount. The results of using a square wave restagger in the calculations can be seen in figure 4.12. The figure shows that with the 10 degree square wave restaggering it is possible to reduce the

velocity non-uniformity by a factor of two.

4.3) Baseline Compressor Behaviour

The compressor was run with the distortion screen installed and uniform IGV stagger angle to find the baseline response. The characteristics with and without distortion are shown in figure 4.13. The pressure rise at stall is 7.9% lower and the stall flow coefficient decreased from 0.38 to 0.37. The drop in pressure rise is to be expected as a result of the total pressure inlet distortion.

The velocity profiles for the distorted flow operating conditions show a more pronounced effect (Figures 4.14 and 4.15). For all flow coefficients the shape of the profiles are similar and follow that of the total pressure profile.

The large change in flow coefficient at the 0 degree position can be explained by the presence of one of the three supporting struts which replaces the IGV at this location. This large spike appears in the distorted flow, as the swirl introduced by the inlet distortion leads to a non-uniform incidence angle on the IGVs around the circumference. At this larger, non-uniform incidence angle the strut will therefore have a stronger influence on the local flow coefficient.

The non-uniformity in the inlet velocity is measured using three methods. The first method is the rms value, the second is the sum of the absolute values of the difference between the average and local flow coefficient and the third

is a Fourier analysis of the velocity profile showing the magnitude of the first three coefficients. Using these measures of non-uniformity the experimental data shows a trend opposite to that of the theoretical calculations (Figure 4.16 and 4.17). The velocity distortion increased towards lower flow coefficients for the theoretical model, while the distortion becomes more severe for higher flow coefficients in the experiment.

This change in behaviour is thought to be due to the setup of the compressor. Due to the separation between the rotor and the stationary blade rows the behaviour of the compressor has similarities to that of an isolated blade rotor. Using an actuator disc model of an isolated rotor the trend observed in the experiment can be predicted. As the calculations show (Figure 4.18) the velocity non-uniformity, in this case the maximum amplitude of a sinusoidal velocity distortion, will increase for higher flow coefficients. The theory therefore confirms the trend observed in the experiment. This change in behaviour will modify the magnitude of the individual distortions, but it does not effect the control scheme otherwise.

4.4) Restaggered Compressor Behaviour

With the restagger implemented the same sets of data were then taken to determine the improvement in performance. The average performance given by the speedline is shown in Figure 4.19. The stall pressure rise is now 0.38 compared

to the baseline 0.36 and the stall flow coefficient moved from 0.37 to 0.38. The loss in pressure rise is smaller than in the uncorrected case. The restaggering of the IGVs has brought the flow coefficient at stall back to the undistorted $\phi = 0.38$.

The changes in the pressure and velocity profiles show this improvement of the flow more clearly. The static pressure is decreased in the region where the vanes are opened relative to the uniform stagger setup (Figures 4.20). This leads to an increase of the velocity and thus a reduction of the distortion for all flow coefficients. The non-uniformity of the velocity profiles in the restaggered setup (Figures 4.21 and 4.22) shows a change from the baseline case, but a direct comparison is difficult due to the non-uniformities in the profiles.

A more detailed examination of the restaggered profiles shows a large increase in velocity in the region between 250 and 290 degrees, as the calculations for the square wave restagger had predicted. This 'spike' is the result of two side effects of the restagger square wave restagger. The restaggering provides too much correction here. The static pressure is reduced even though this section is not in a low total pressure region, thus leading to an increases in velocity.

There is also an effect due to the spacing between the blade rows. As the actuator disc calculations had shown the spacing would lead to a correction that would be larger than the calculated correction for zero spacing, in the direction

of the swirl induced by the IGVs. The spike is more extreme in the experiment due to the abrupt change in stagger at this location from 5 to 25 degrees. The spike could therefore be removed if the restagger were implemented interactively, using a measurement of the local flow velocity to restagger the IGVs in that region.

The increases in the flow coefficient at 135, 200 and 360 degrees in figures 4.21 and 4.22 are again a result of the supporting struts.

The comparison of the criteria for distortion magnitude show a clearer decrease of a factor of two in the velocity non-uniformities for all flow coefficients (Figure 4.23 and 4.24). For the higher flow coefficients the restagger is not as effective as for the lower flow coefficients, as it was designed for a flow coefficient of $\phi = 0.45$. A comparison of the phase of the first three harmonics (Figure 4.25) shows only small changes in the phase of the harmonics.

4.5) Limitations

These results of the response of the compressor to the distortion and the resulting restaggering show some of the limits of the basic scheme.

The exit static pressure profile does not agree with the uniform pressure assumption of the model (Figure 4.26). This non-uniformity existed with and without the distortion, and the conclusion is that it is due to the compressor and

not due to the restaggering of the IGVs.

The shift of the static pressure profile in direction of rotor rotation relative to the original total pressure distortion is ignored in the linear model, which assumes no spacing between the blade rows. This together with the sudden change in stagger angle at the interface of the two regions leads to an interaction of the two sections not included in the parallel compressor model.

Chapter 5 Conclusions and Recomendations for Future Work

5.1) Conclusions

The results of the implementation of the non-axisymmetric stagger are encouraging even given the very non-ideal test conditions. They show that it is possible to reduce the velocity distortion at the compressor face by a factor of two with an IGV restagger of 10 degrees. A setup with closer more typical spacing between the blade rows and aerodynamically improved IGVs, typical of current axial compressors, should increase the ability to reduce velocity distortions and extend the method to even larger inlet total pressure distortions.

Non-axisymmetric restaggering also reduced the loss in pressure rise due to the inlet total pressure distortion.

5.2)Recomendations for Future Work

The restaggering required of the IGVs is in the range possible in current engines. The possibility of implementing this method opens further questions on overall engine performance that need to be investigated.

The ability of the scheme to adapt to different inlet distortions plays a role in its usefulness. If each blade has to be controlled independently to achieve the reduction in velocity non-uniformity the improvements will be much

smaller, due to the weight and complexity of the actuators, than if sectors of 60 to 90 degrees can be restaggered by a single actuator. A future investigation would therefore test a compressor with inlet total pressure distortion and a restagger in a certain section with varying phase between the two, to determine how accurately the restaggering has to be positioned to obtain a desired decrease in flow non-uniformity.

Similarly the number of sensors required to determine the location and magnitude of the distortion will depend on the level of accuracy needed to show an improvement in compressor behaviour. Here the work would concentrate on the number of probes required to locate the inlet distortion.

The implementation of this method in an engine would then require a quick method, such as a lookup table, that would specify the amount of restagger required for each sector according to the extend and magnitude of the distortion as well as the location of the current operating point on the speedline. Future work in this area would deal with the amount of time required between the sensing of an inlet distortion and the repositioning of the IGVs.

Before this method can be applied to actual compressors further work will have to be done to compare the relative gains of implementing this method instead of improvements gained by an additional compressor stage and the amount of sensing required to make the restaggering an efficient method of improving distortion tollerance.

REFERENCE

1) Seymore, J. C., 'Aircraft Perormance Enhancement with Active Compressor Stabilization',MIT Thesis Sept 1988

2) Mazzaway, R. S., 'Multiple Segment Parallel Compressor Model for Circumferential Flow Distortion', Engineering for Power, Vol. 99 No. 2, April 1977

3) Stenning, A. H., 'Inlet Distortion Effects in Axial Compressors', Journal of Fluid Engineering, Vol. 102, March 1980

4) Reid, C., 'The Response of Axial Flow Compressors to Intake Flow Distortion', ASME Paper 69-GT-29, 1969 ASME Gas Turbine Conference

5) Hynes, T. P. and Greitzer, E. M., 'A Method of Assessing Effects of Circumferential Flow Distortion on Compressor Stability', ASME Journal of Gas Turbines and Power,

6) Hynes, T. P., Chue, R., Greitzer, E. M. and Tan, C. S., 'Calculation of Inlet Distortion Induced Compressor Flow Field Instability', AGARD Conference Proceedings No. 400, 'Engine Response to Distorted Inflow', March 1987

7) Epstein, A. H., ''Smart' Engine Components: A Micro in Every Blade?', Aerospace America, Vol. 24, January 1986

8) Chen, G. T., 'Active Control of Turbomachinery Instability - Initial Calculations and Results', MIT Thesis August 1987

9) Raw, J. A., and Weir, G. C., 'The Prediction of Off-Design Characteristics of Axial and Axial/Centrifugal Compressors', SAE Technical Paper 800628, April 1980

10) Rannie, W.D. ,'The Axial Compressor Stage', Section F of 'Aerodynamics of Turbines and Compressors', Princeton University Press, 1964

11) Bruce, E. P., 'Design and Evaluation of Screens to Produce Multi-Cycle 20% Amplitude Sinusoidal Velocity Profiles', AIAA Paper No. 74-623, AIAA 8th Aerodynamic Testing Conference, July 1974

Appendix Actuator Disc Modeling

As the model used in the origional calculations assumed a compressor with closely spaced blade rows the changes due to the large seperations in the experimental machine had to be investigated seperately. Actuator disc theory allows a quick and simple estimation of the trends introduced by the spacing.

The first set of calculations are an estimate of the change in ability to correct the flow due to the seperation between the blade rows. The flow field is divided into three regions, the flow upstream of the IGV plane, the flow in the gap between IGVs and rotor, and the flow downstream of the stator. The rotor and stator are lumped into one disc, as all the restaggering occours in the IGV blade row.

The flow in the three regions is then governed by

$$\nabla^2\Psi_1 = -\omega_1 = L\, e^{in\theta}$$

$$\nabla^2\Psi_2 = -\omega_2 = M\, e^{-in \tan \beta_2 (x/R) + in\theta} \qquad (A-1)$$

$$\nabla^2\Psi_3 = -\omega_3 = N\, e^{-in \tan \beta_3 (x/R) + in\theta}$$

respectively. The magnitude of L is determined by the magnitude of the inlet distortion and M and N are determined by the loading on the blade rows.

The stream functions that satisfy these equations are

$$\Psi_1 = A\, e^{in\theta + nx/R} + B\, e^{in\theta - nx/R} + W\, e^{in\theta}$$

$$\Psi_2 = C\, e^{in\theta + nx/R} + D\, e^{in\theta - nx/R} + E\, e^{in(\theta - x/R \tan \alpha_2)} \qquad (A-2)$$

$$\Psi_3 = F\, e^{in\theta + nx/R} + G\, e^{in\theta - nx/R} + H\, e^{in(\theta - n/R \tan \alpha_3)}$$

The magnitude of the constants A through H are determined by the boundary conditions at $x = \pm \infty$ and at the two blade rows $x = 0, h$.

at $x = -\infty$ Ψ is bounded => B = 0

at $x = \infty$ Ψ is bounded => F = 0

At each of the blade rows three boundary conditions have to be met. Contenuity has to be satisfied, the flow leaving angle is specified by the blade setting and the pressure rise is given by the compressor characteristic.

at $x = 0$

$$A + W = C + D + E$$

$$-i \tan \alpha_1 \; A = C - D - i \tan \alpha_2 E \qquad (A-3)$$

$$\frac{1}{R}\left(\frac{\partial p_2}{\partial \theta} - \frac{\partial p_1}{\partial \theta}\right) = \frac{1}{2}\rho \left\{\left[2U_1 \frac{\partial U_1}{\partial \theta} + 2V_1 \frac{\partial V_1}{\partial \theta}\right] c_p + \left[U_1^2 + V_1^2\right] \frac{\partial c_p}{\partial \theta}\right\}$$

at $x = h$

$$C\, e^{inh/R} + D\, e^{-inh/R} + E\, e^{-inh/R} \tan \alpha_2 = G\, e^{-inh/R} + H\, e^{-inh/R} \tan \alpha_3 \qquad (A-4)$$

$$in \frac{\tan \alpha_2}{R} \left(C\, e^{inh/R} + D\, e^{-inh/R} + E\, e^{-inh/R} \tan \alpha_2\right) = -\frac{n}{R} G\, e^{-nh/R} + H\, e^{-nh/R} \tan \alpha_3$$

$$\frac{1}{R}\left(\frac{\partial p_3}{\partial \theta} - \frac{\partial p_2}{\partial \theta}\right) = \frac{1}{2}\rho \left\{\left[2U_2 \frac{\partial U_2}{\partial \theta} + 2V_2 \frac{\partial V_2}{\partial \theta}\right] c_p + \left[U_2^2 + V_2^2\right] \frac{\partial c_p}{\partial \theta}\right\}$$

the pressure depedency can be removed from the dynamic equations by substituting the momentum equation

$$U\frac{\partial U}{\partial x}+\frac{V\partial V}{R_{\partial\theta}}=\frac{1}{\rho R}\frac{\partial p}{\partial\theta} \qquad \text{(A-5)}$$

The velocities are then expressed in the streamfunctions and the equations linearized by dropping all second order terms. The resulting 6 x 6 system can then be evaluated for any desired inlet distortion or IGV blade distribution.

The other application is the calculation of the effect of an isolated rotor on a velocity distortion. In this case the flowfield is divided into an upstream and downstream region.

$$\nabla^2\Psi_1 = -\omega_1$$

$$\nabla^2\Psi_2 = -\omega_2 \qquad \text{(A-5)}$$

In this case the pararmeter was the flow coefficient of the compressor. As a result of this the pressure rise of the blade row had to be included as a function of the flow coefficient. The model uses a curve-fit of the nominal experimental speedline for this, as the calculations are only intended to show the trend in the magnitude of the velocity distortion. The change in pressure rise around the circumference due to the velocity non-uniformity is acounted for by using the slope of the characteristic at the average flow coefficient. The flow direction in the downstream region is now also dependent on the flow coefficient, as the relative leaving angle is asumed to be constant.

Applying the boundary conditions at x = and at x = 0 and performing the same substitutions as before leads to a 3

x 3 system that can be solved to find the effect of the rotor.

	IGV	Rotor	Stator
Hub Diameter (mm)	444	444	444
Casing Diameter (mm)	597	597	597
Number of Blades	46	44	45
Chord (mm)	33	38	38
Solidity at Midspan	0.9	1.0	1.0
Aspect Ratio	2.2	1.9	1.9
Camber (deg)	12	25.5	30.0
Midspan Stagger (deg)	15	28.7	45.0
Blade Clearance (mm)	1.6	0.8	1.5

Table 2.1
Compressor Geometry

Sector (deg)	Loss Coefficient Pt/.5 Rho Cx^2
-90 to -70	1.02
-70 to -30	1.34
-30 to 30	1.72
30 to 70	1.34
70 to 90	1.02
90 to -90	0.32

Table 3.1

Distortion Screen Total Pressure
Loss Coefficient

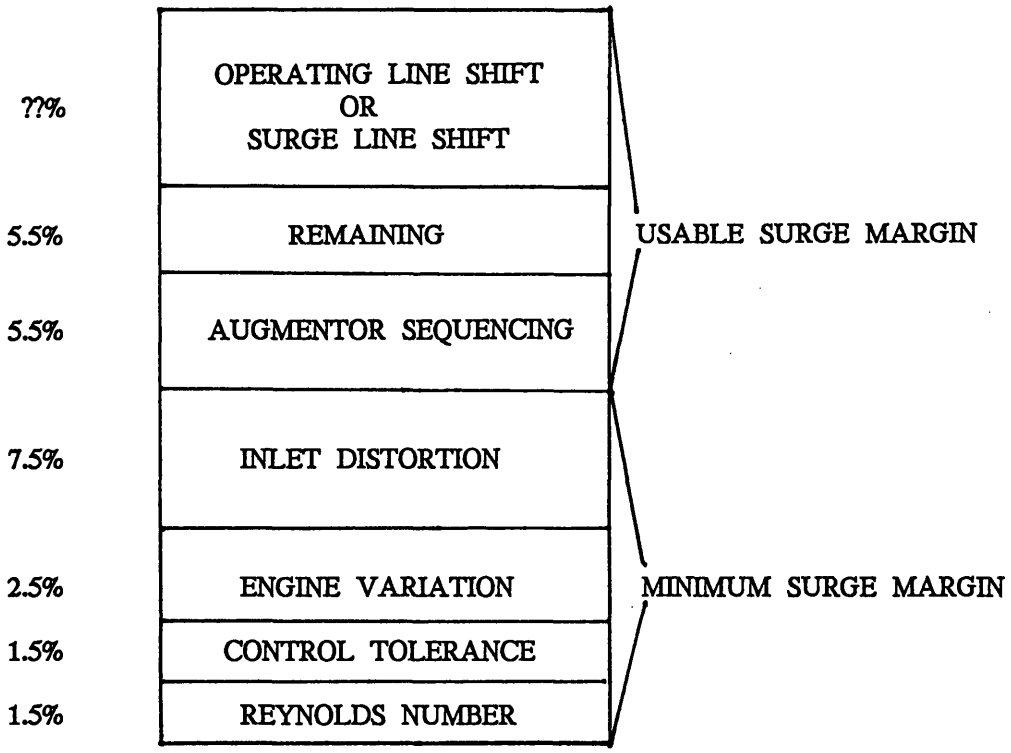

Fig. 1.1 Typical Allocation of Required Surge Margin [1]

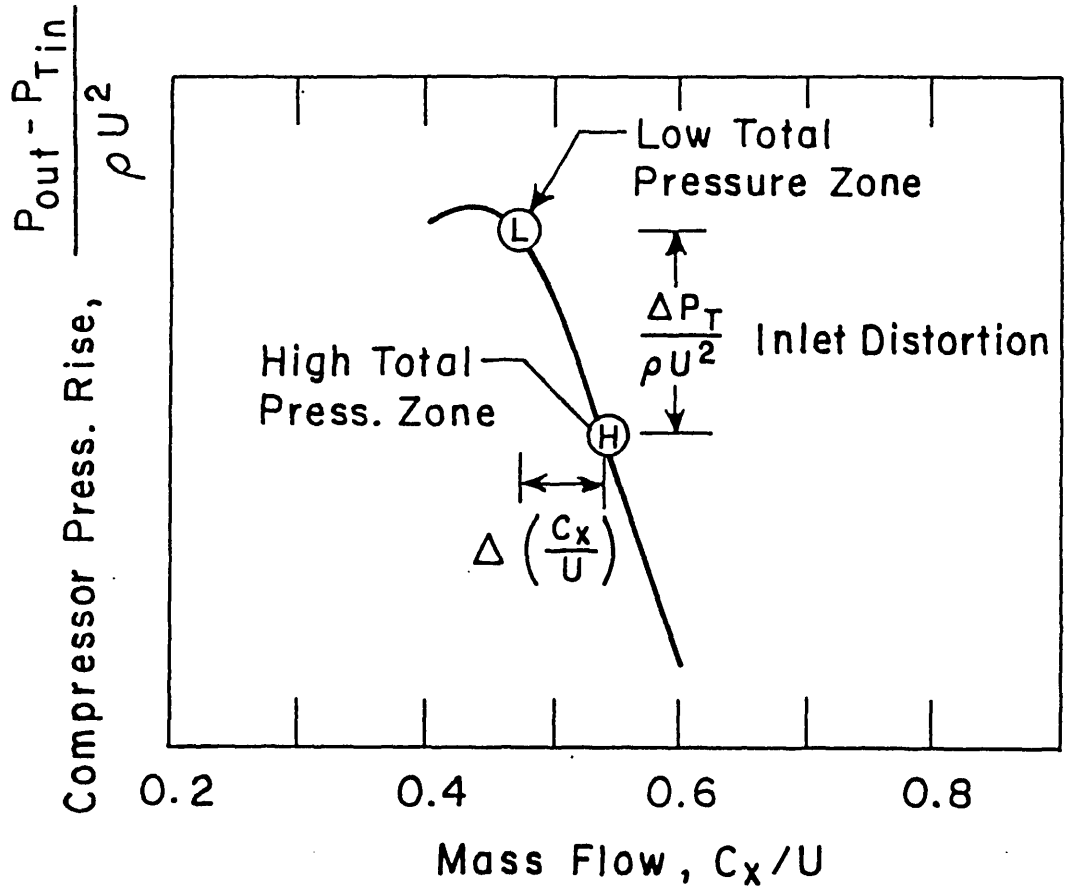

Fig. 1.2 Parallel Compressor Description of Response to Circumferrential Distortion

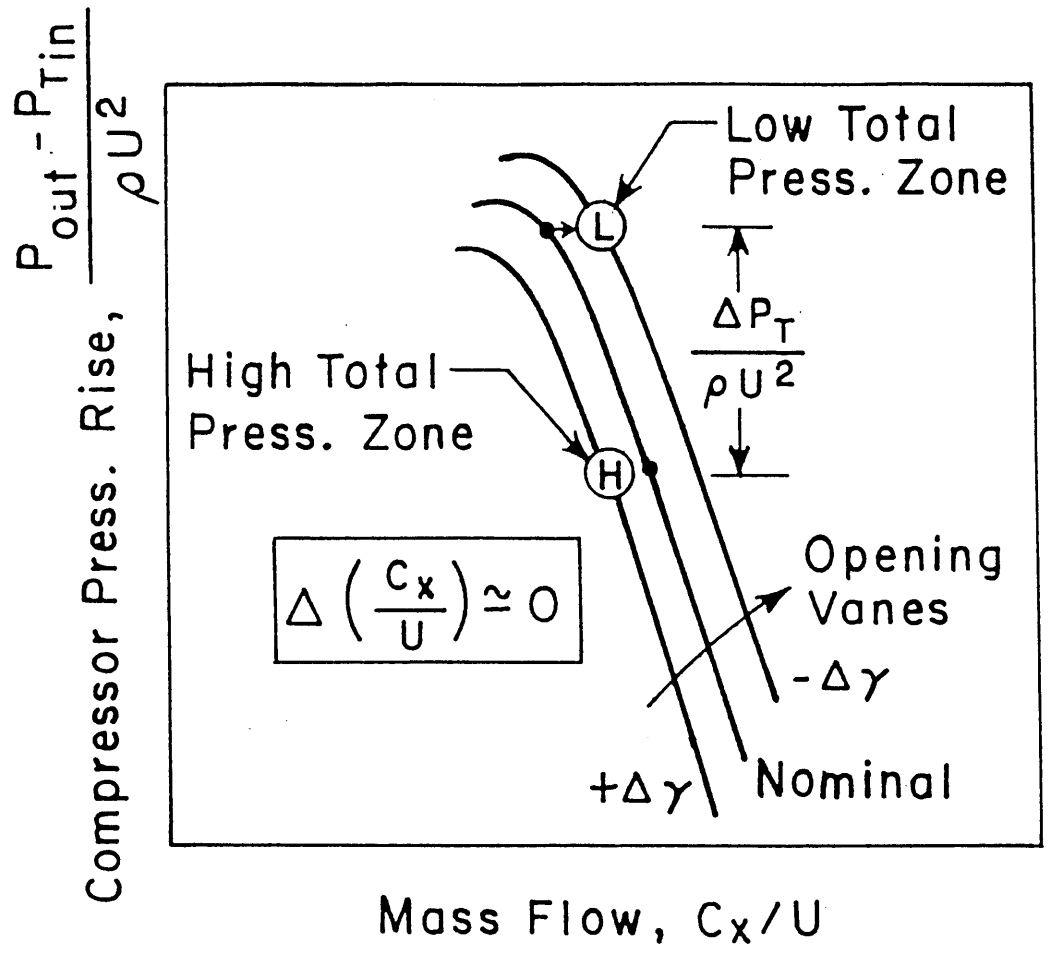

Fig. 1.3 Effect of Non-Axisymmetric Vane Stagger on Compressor Response to Total Pressure Distortion

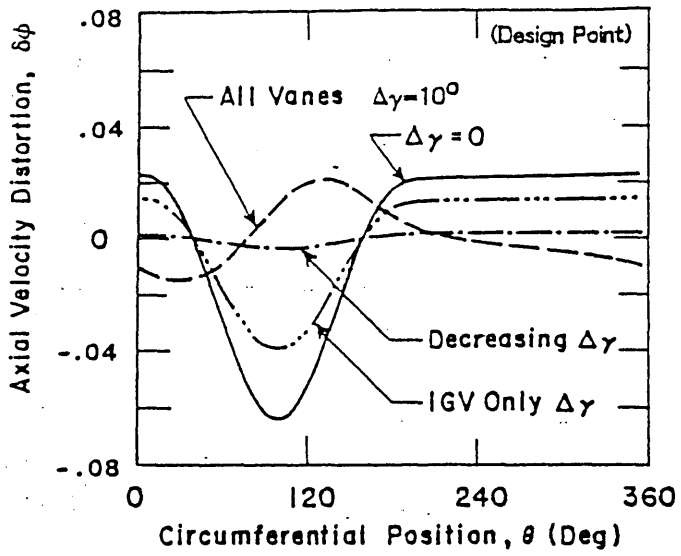

Fig. 2.1 Three Stage Compressor Response to Three Restaggering Schemes [8]

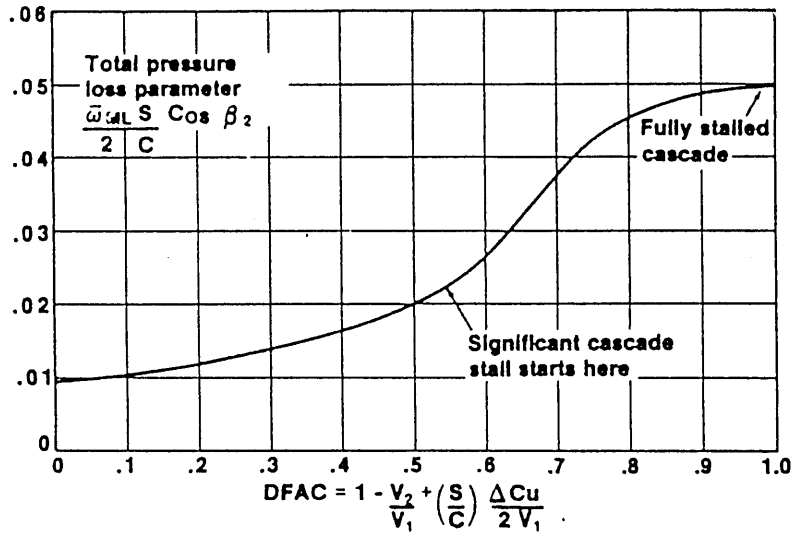

Fig. 2.2 Empirical Curve Relating Loss Coefficient and Diffusion Factor [9]

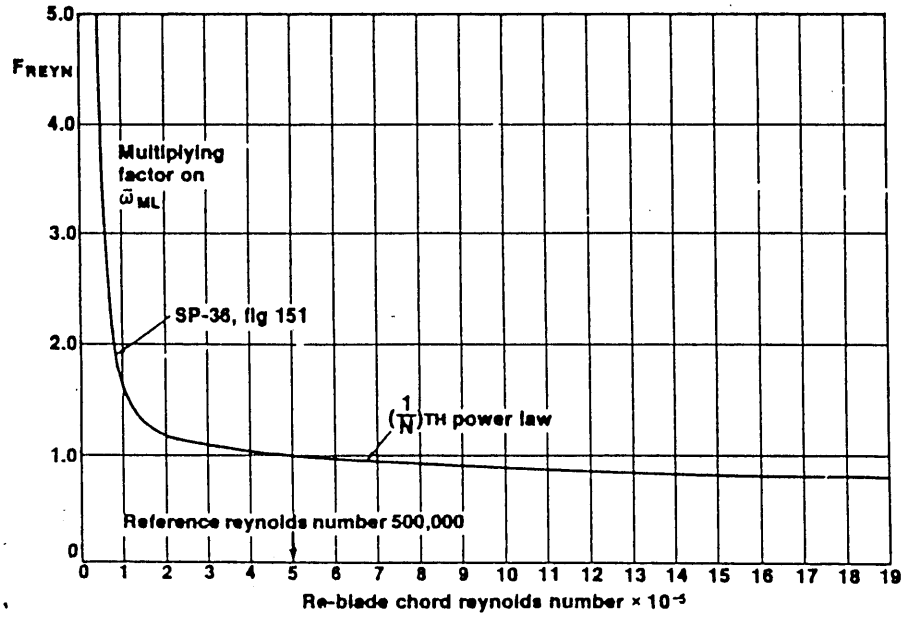

Fig. 2.3 Multiplying Factor on Loss Coefficient as a Function of Diffusion Factor [9]

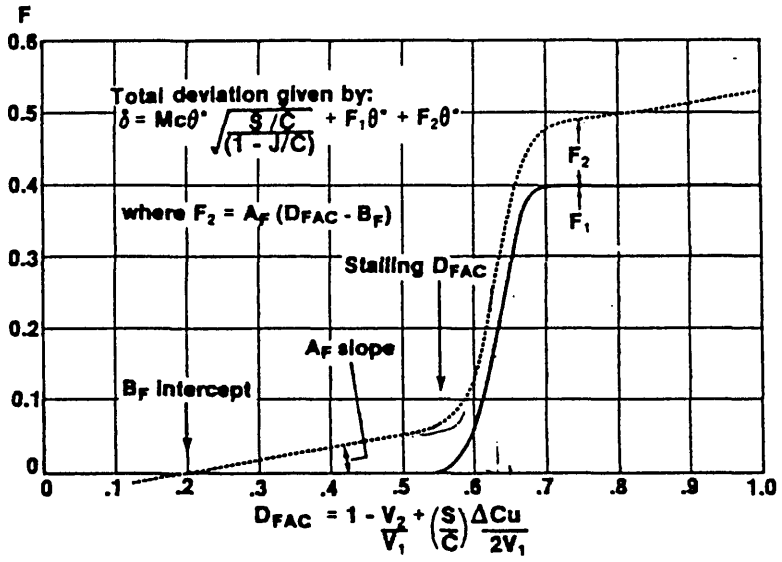

Fig. 2.4 Deviation 'Adder' Applied to Carter's Rule as a Function of Diffusion Factor [9]

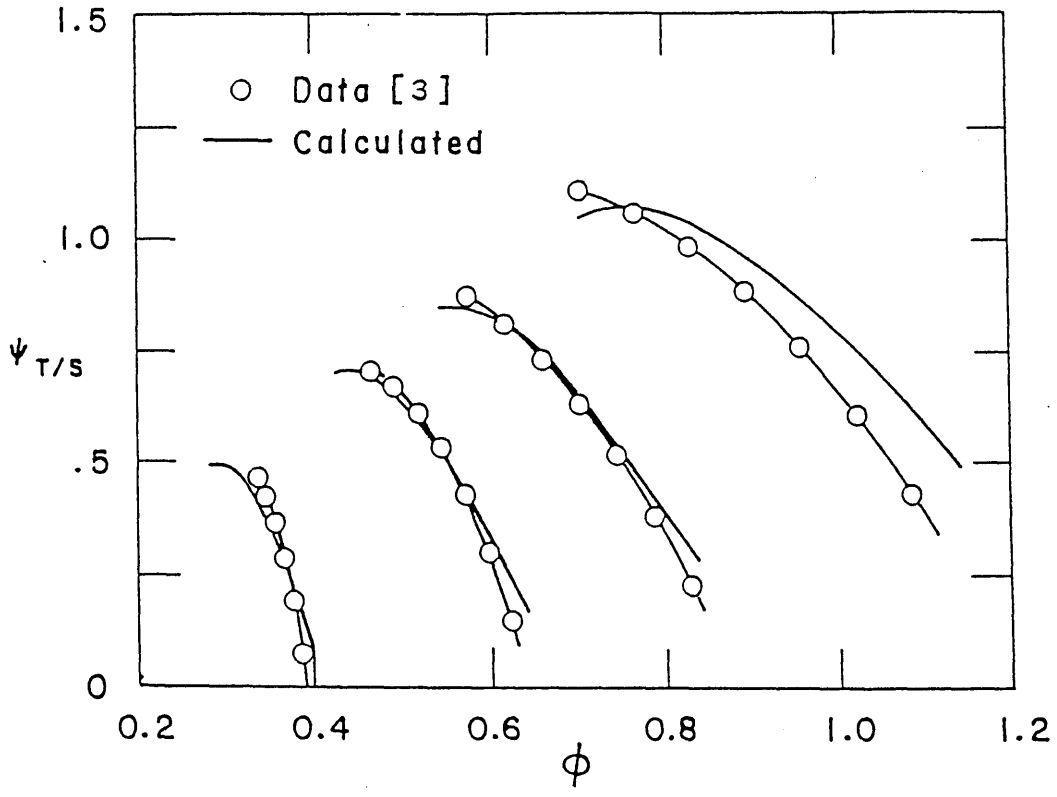

Fig. 2.5 Calculated and Experimental Data for 4 Low Speed Three-Stage Compressors [8]

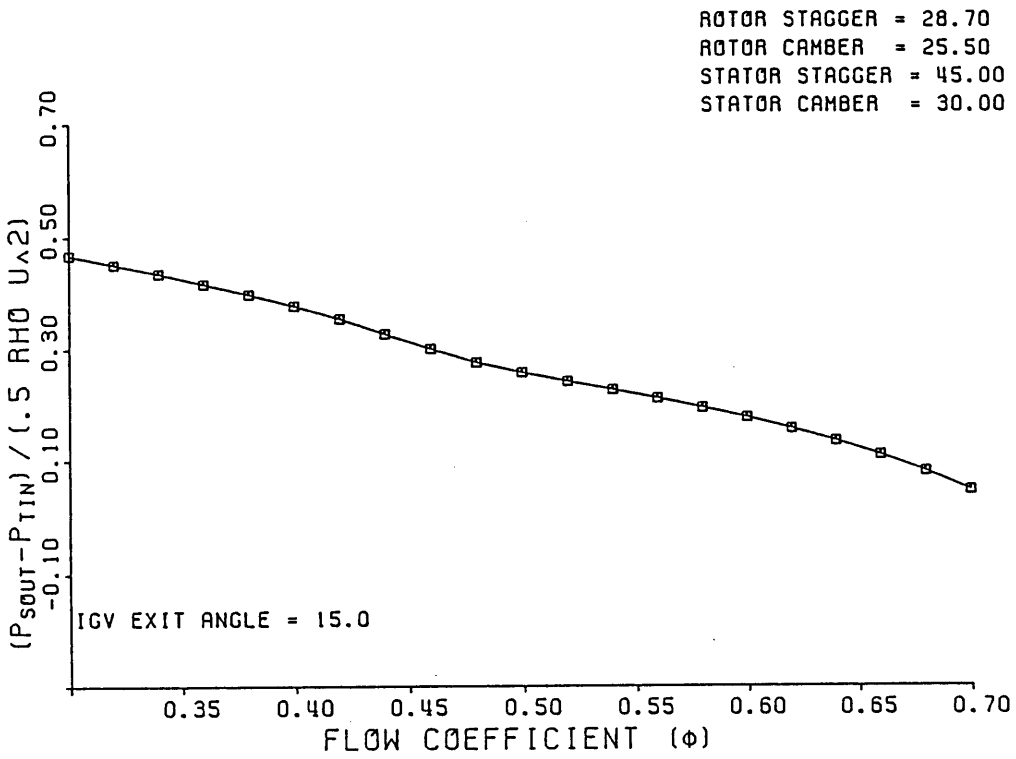

Fig. 2.6 Compressor Speedline for Control Modeling

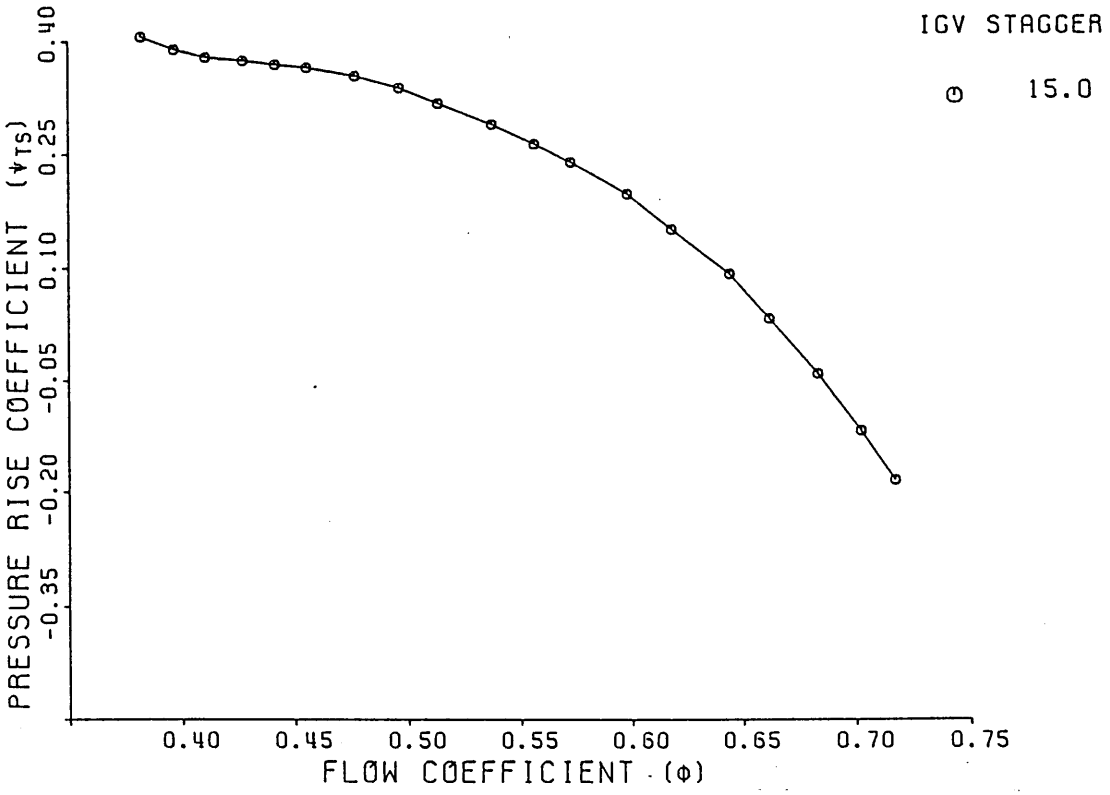

Fig. 2.7 Experimental Speedline

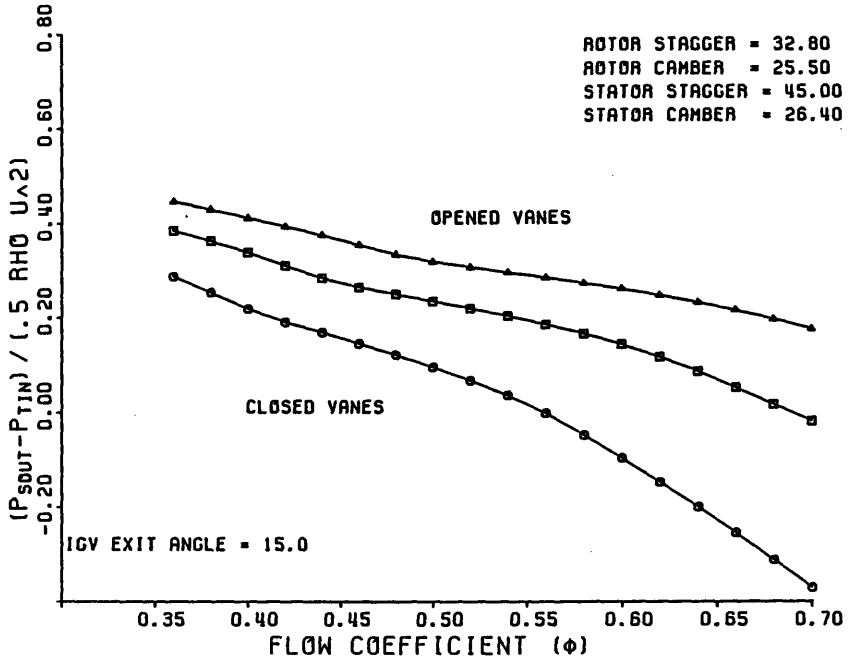

Fig. 2.8 Calculated Compressor Speedlines with a 10 Degree Opening and Closing of IGVs and Stators

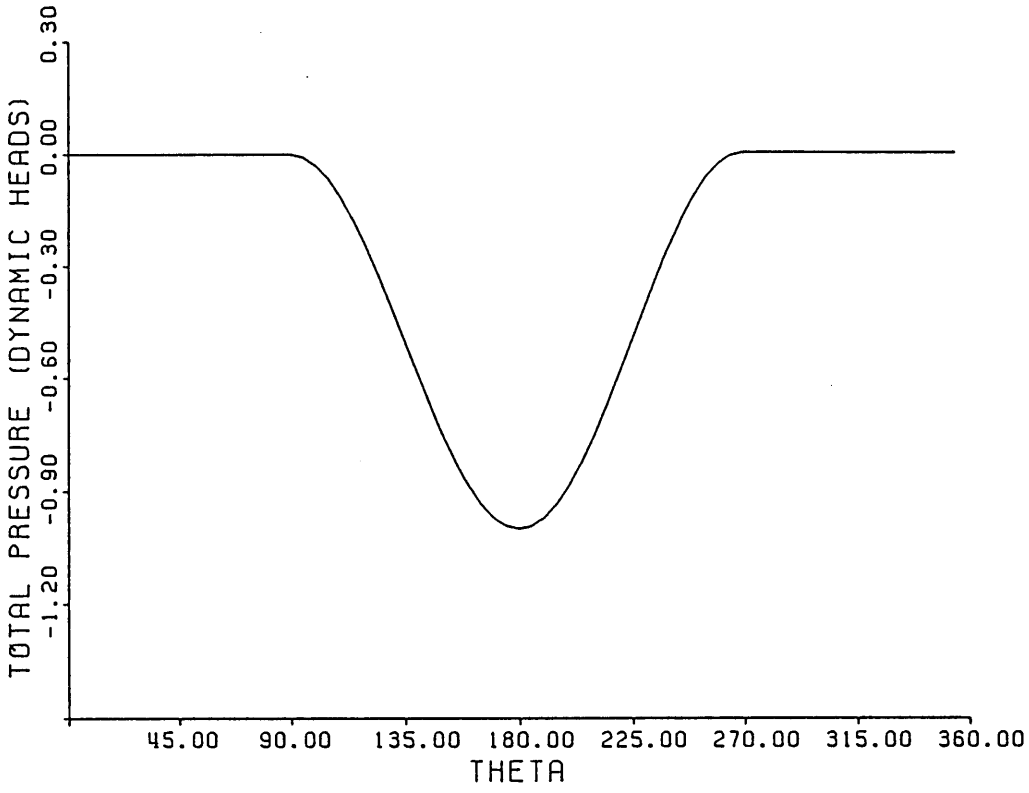

Fig. 2.9 Inlet Total Pressure Distortion Profile

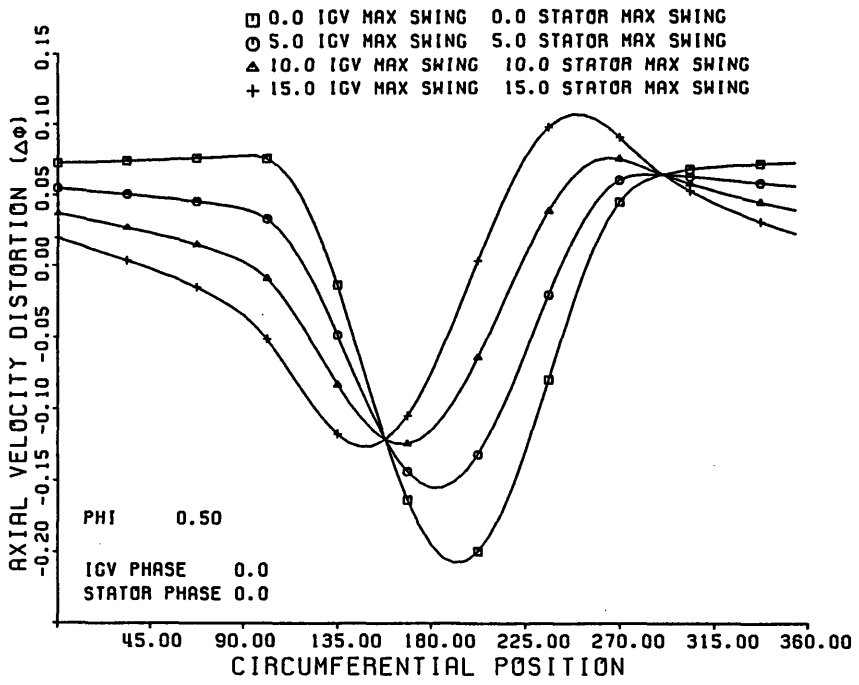

Fig. 2.10 Compressor Response to a 1.0 Dynamic Head Distortion with a 0,5,10,15 Degree Restagger of the IGVs and Stators Near Stall

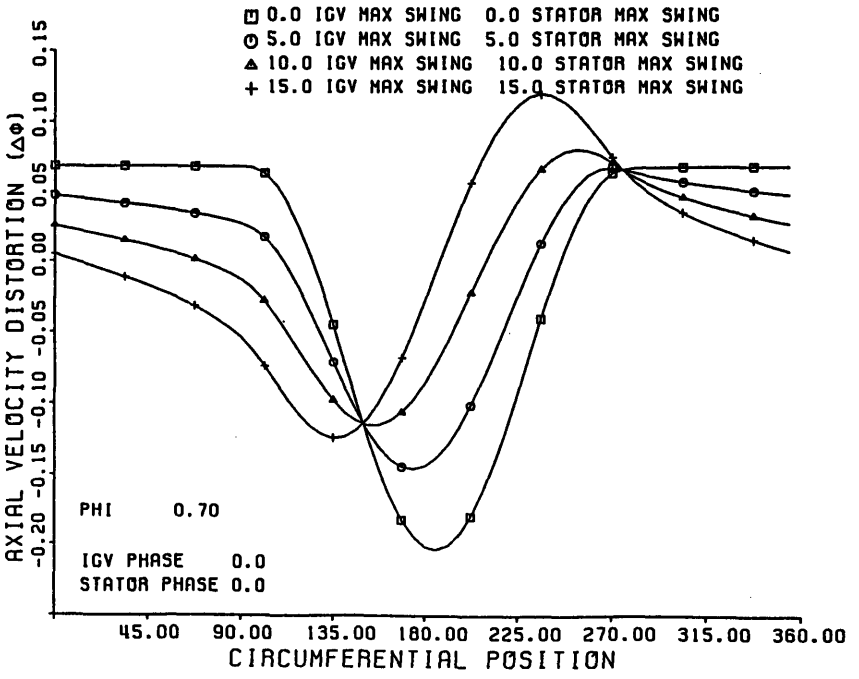

Fig. 2.11 Compressor Response to a 1.0 Dynamic Head Distortion with a 0,5,10,15 Degree Restagger of the IGVs and Stators at Design Flow

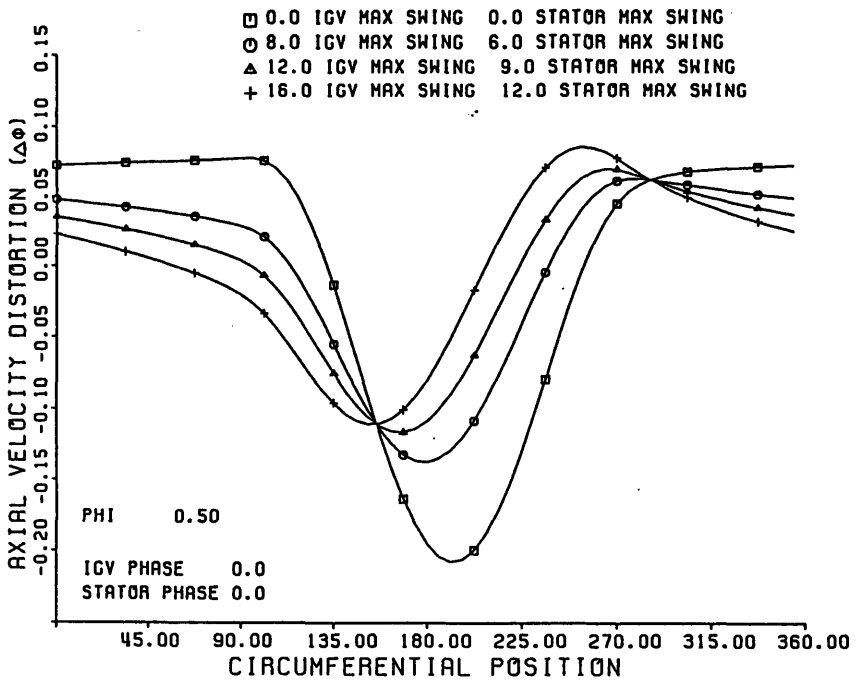

Fig. 2.12 Compressor Response to a 1.0 Dynamic Head Distotrion with a 0,8,12,16 Degree Graduated Restagger of the IGVs and Stators Near Stall

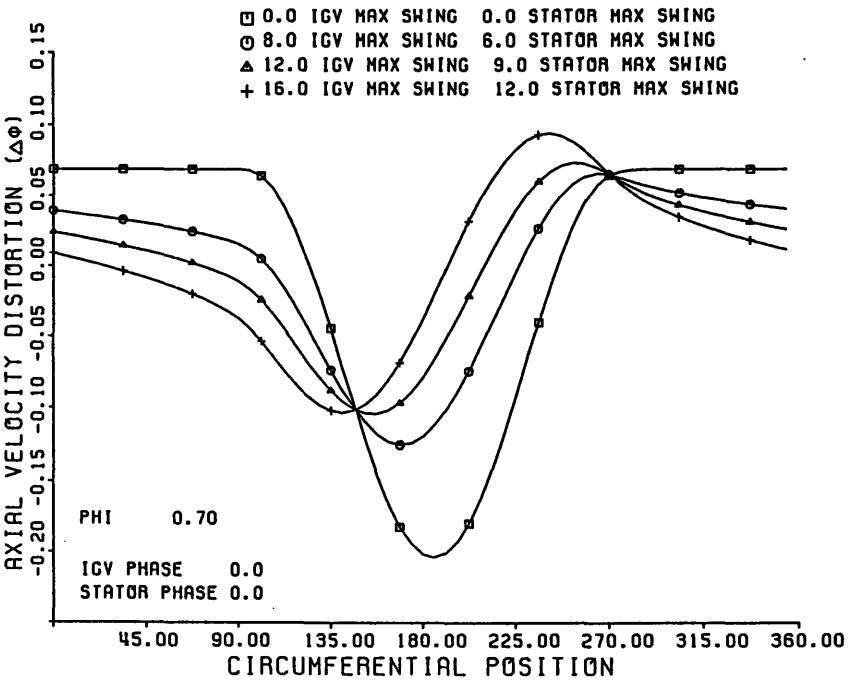

Fig. 2.13 Compressor Response to a 1.0 Dynamic Head Distotrion with a 0,8,12,16 Degree Graduated Restagger of the IGVs and Stators at Design Flow

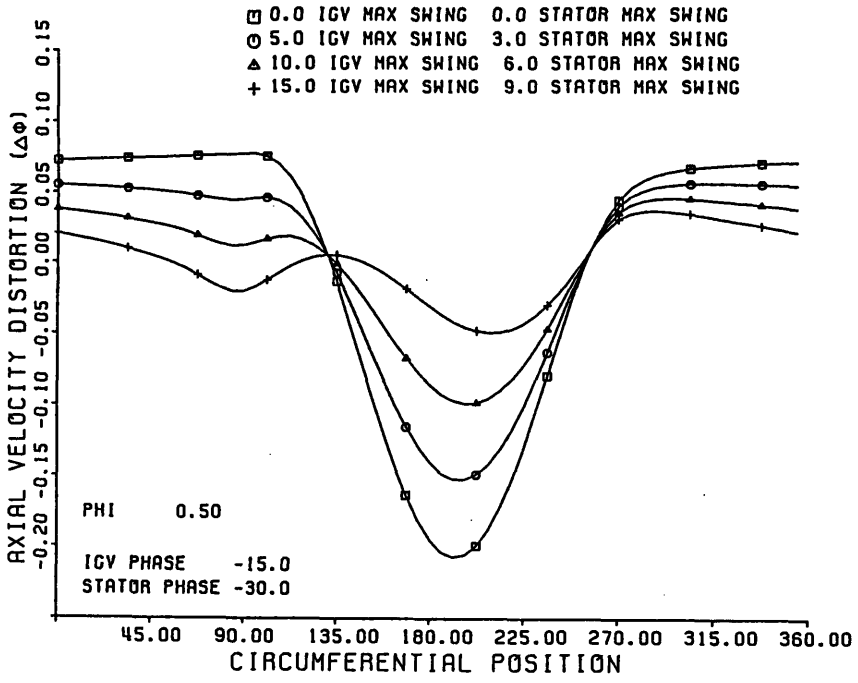

Fig. 2.14 Compressor Response to a 1.0 Dynamic Head Distotrion with a Shifted Graduated Restagger of the IGVs and Stators Near Stall

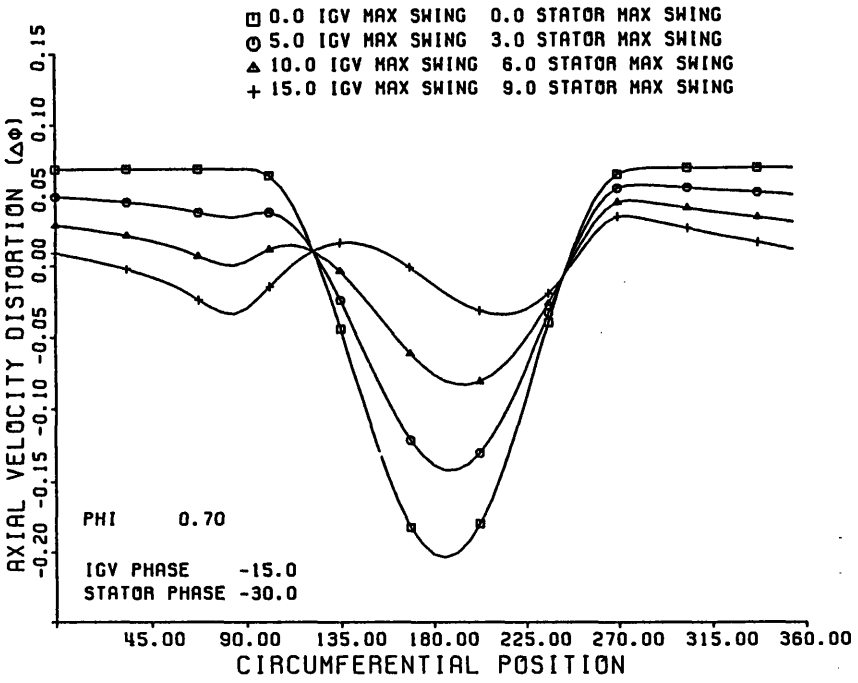

Fig. 2.15 Compressor Response to a 1.0 Dynamic Head Distotrion with a Shifted Graduated Restagger of the IGVs and Stators at Design Flow

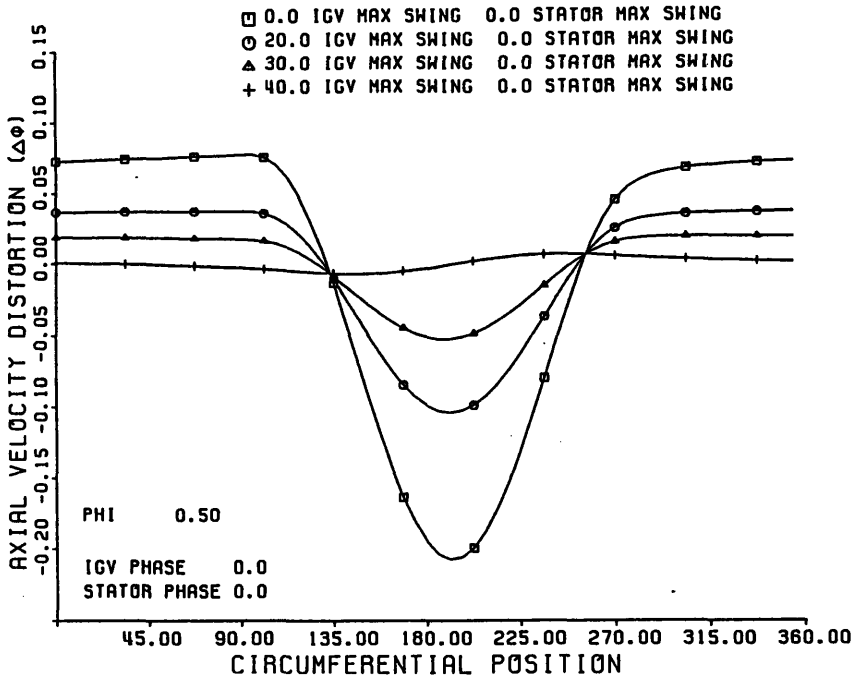

Fig. 2.16 Compressor Response to a 1.0 Dynamic Head Distortion with a 0,20,30,40 Degree IGV Restagger Near Stall

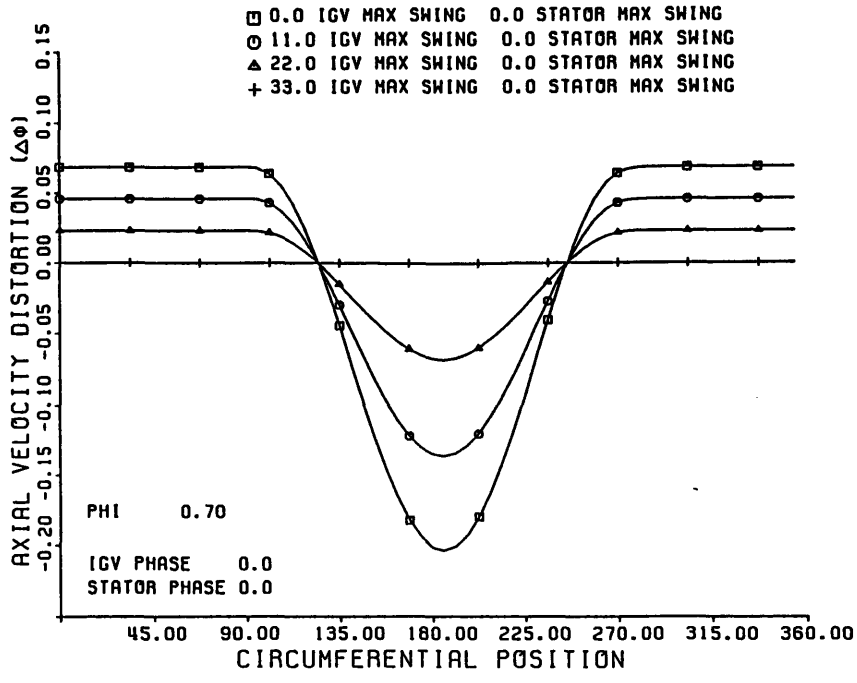

Fig. 2.17 Compressor Response to a 1.0 Dynamic Head Distortion with a 0,11,22,33 Degree IGV Restagger at Design Flow

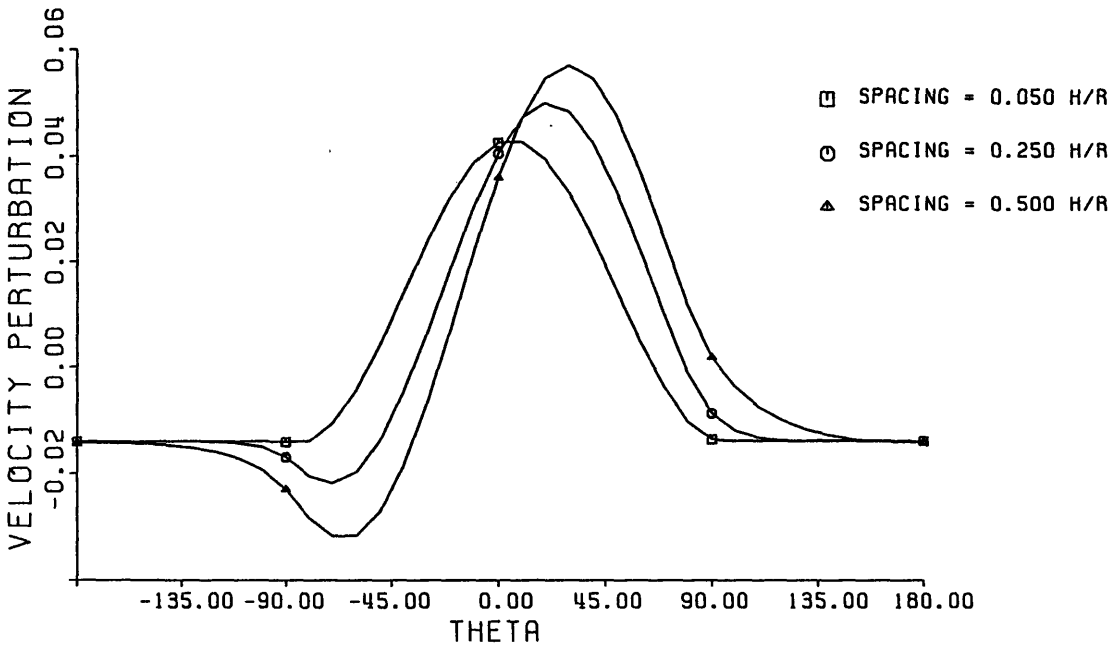

Fig. 3.1 Axial Velocity Perturbation Introduced by a 10 Degree IGV Restagger vs. Blade Row Spacing

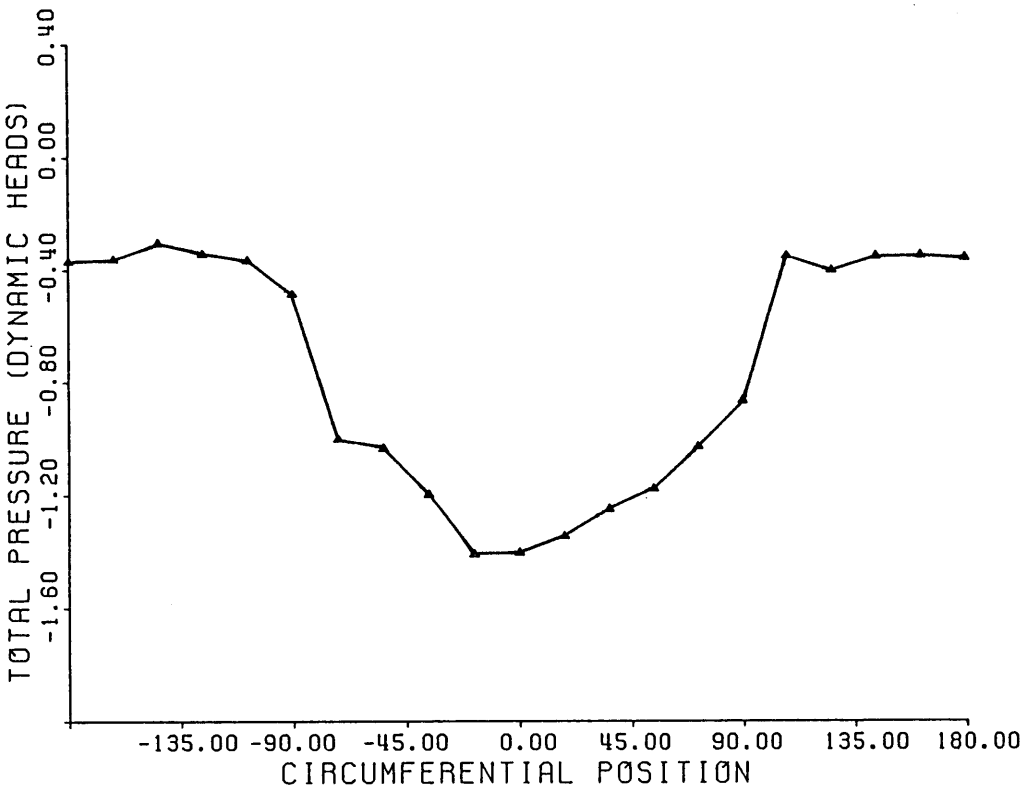

Fig. 3.2 Circumferential Inlet Total Pressure Profile with Inlet Distortion

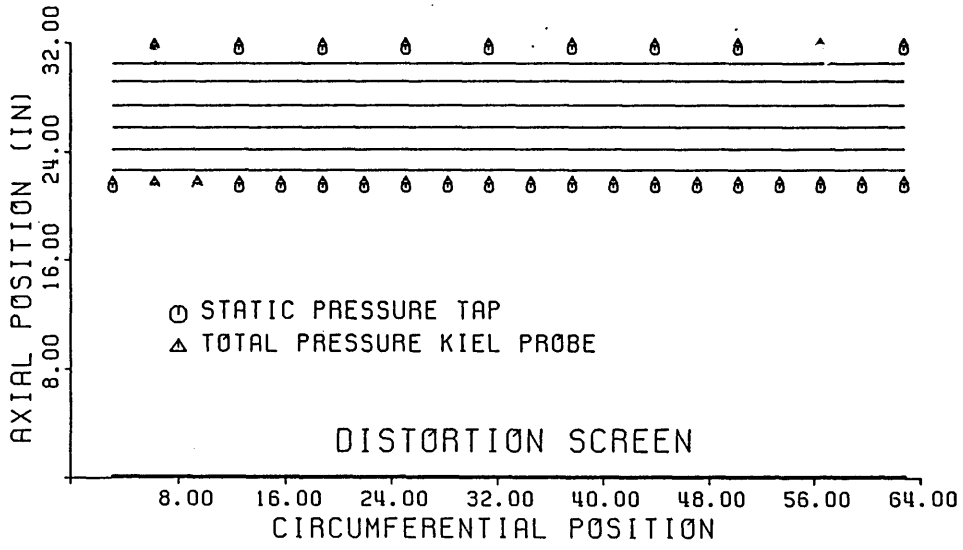

Fig. 3.3 Pressure Instrumentation Layout

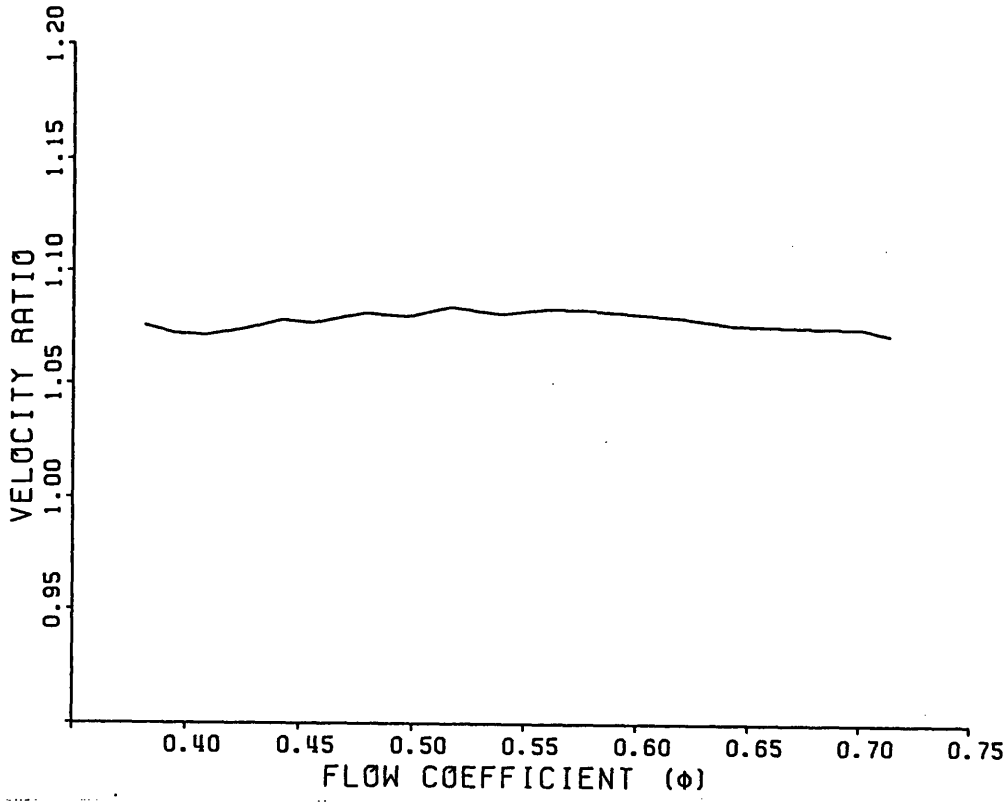

Fig. 3.4 Velocity Measured by Pitot Tube vs. Velocity Measured by Total Pressure Kiel Probes and Static Pressure Taps

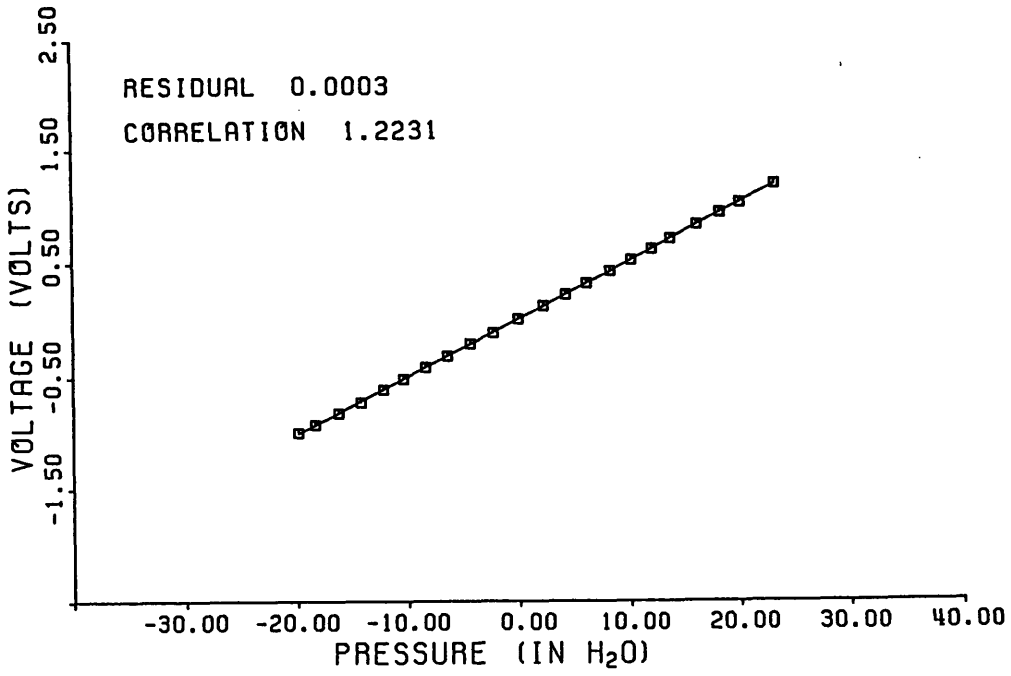

Fig. 3.5 Scannivalve 1 Pressure Transducer Calibration Curve

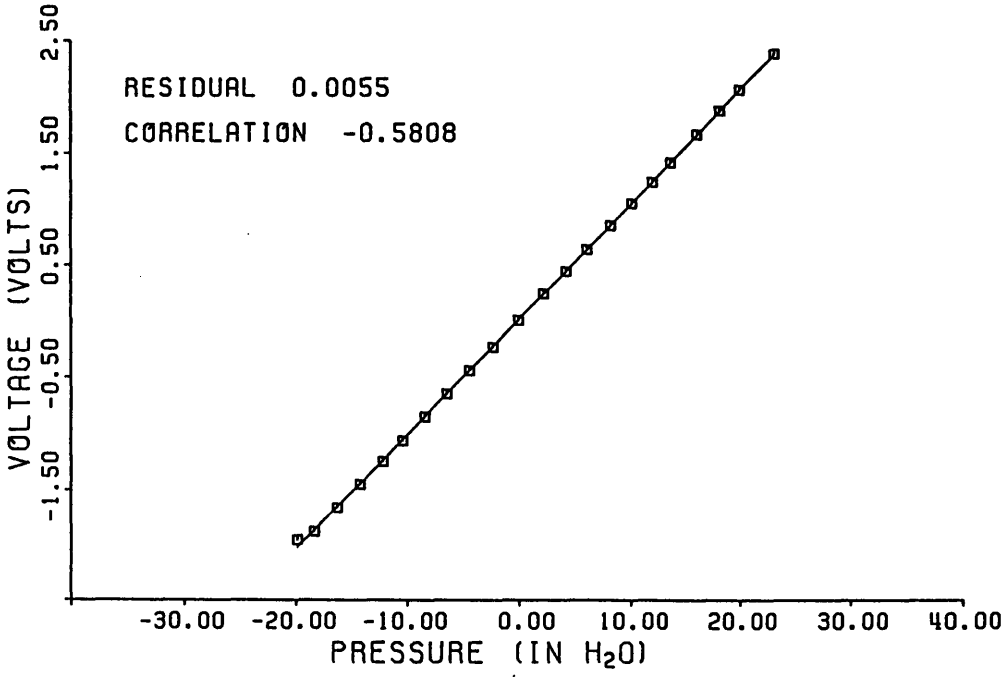

Fig. 3.6 Scannivalve 2 Pressure Transducer Calibration Curve

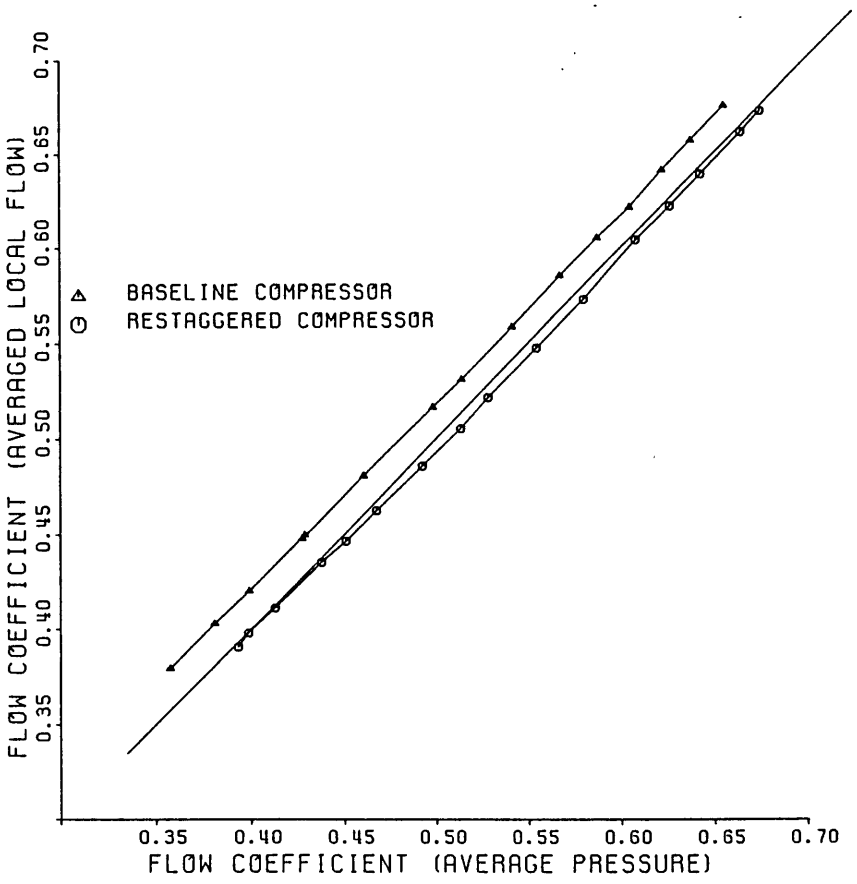

Fig. 3.7 Flow Coefficient from Average Pressure Reading vs Coefficient from Averaged Local Flow

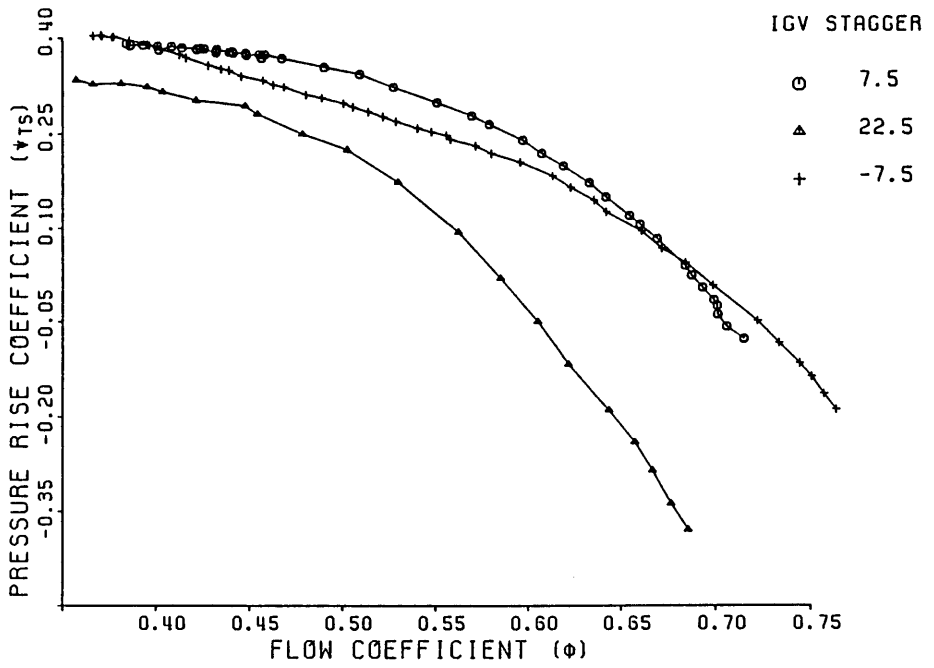

Fig. 4.1 Compressor Speedlines for 7.5, -7.5 and 22.5 Degree IGV Stagger

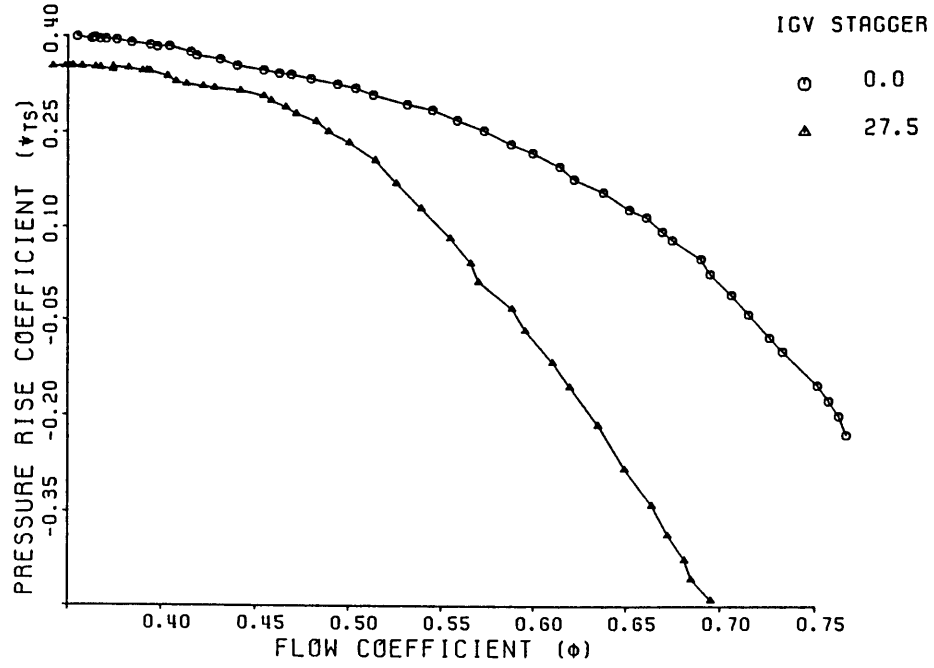

Fig. 4.2 Compressor Speedlines for 0.0 and 27.5 Degree IGV Stagger

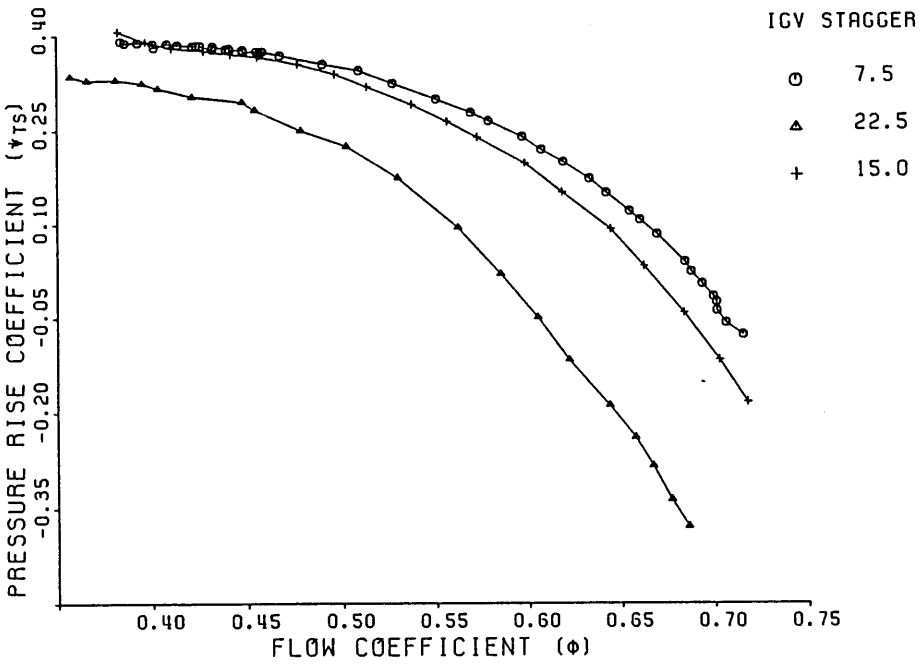

Fig. 4.3 Compressor Speedline for 7.5, 15.0 and 22.5 Degree IGV Stagger

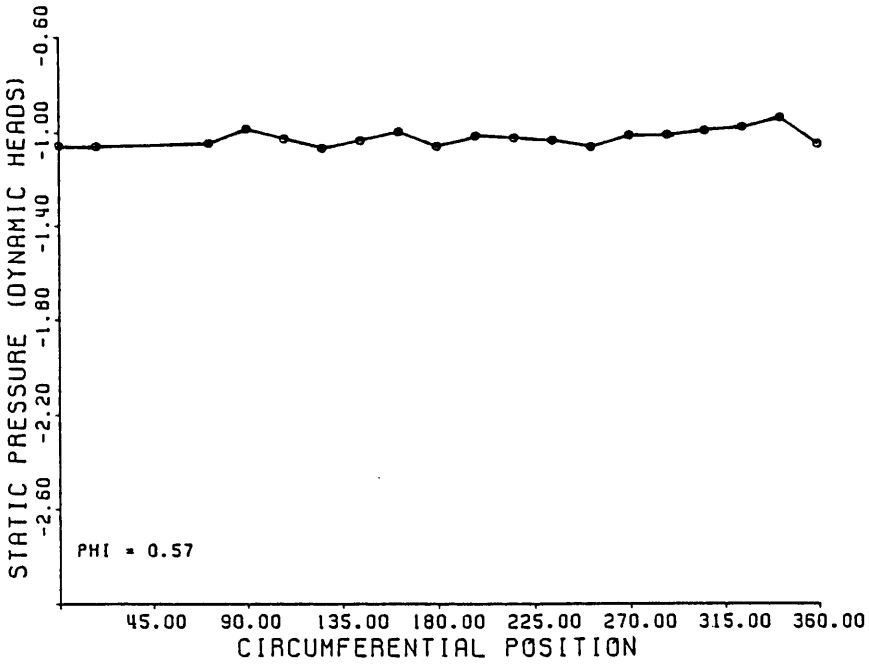

Fig. 4.4 Inlet Static Pressure Profile at Design Flow

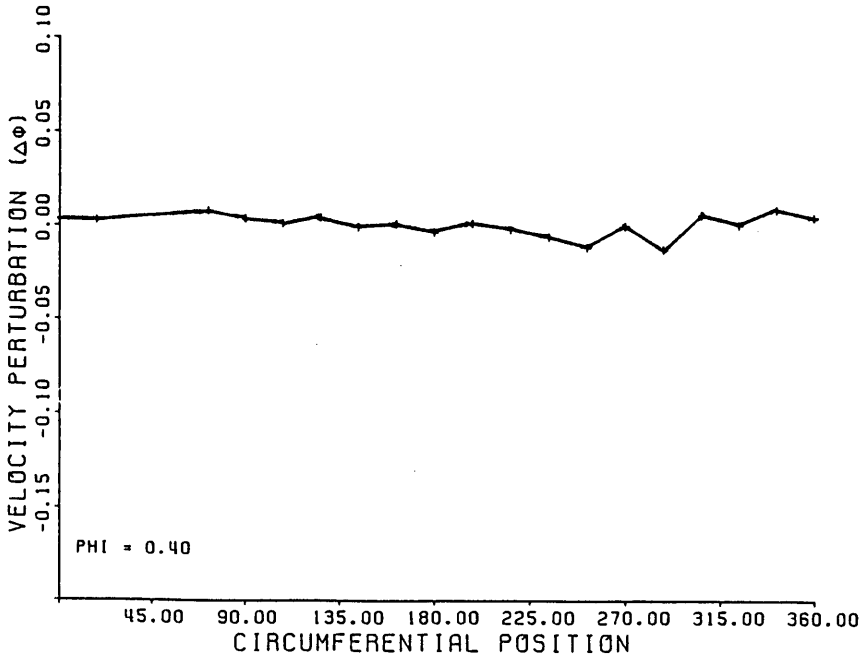

Fig. 4.5 Inlet Velocity Profile Near Stall

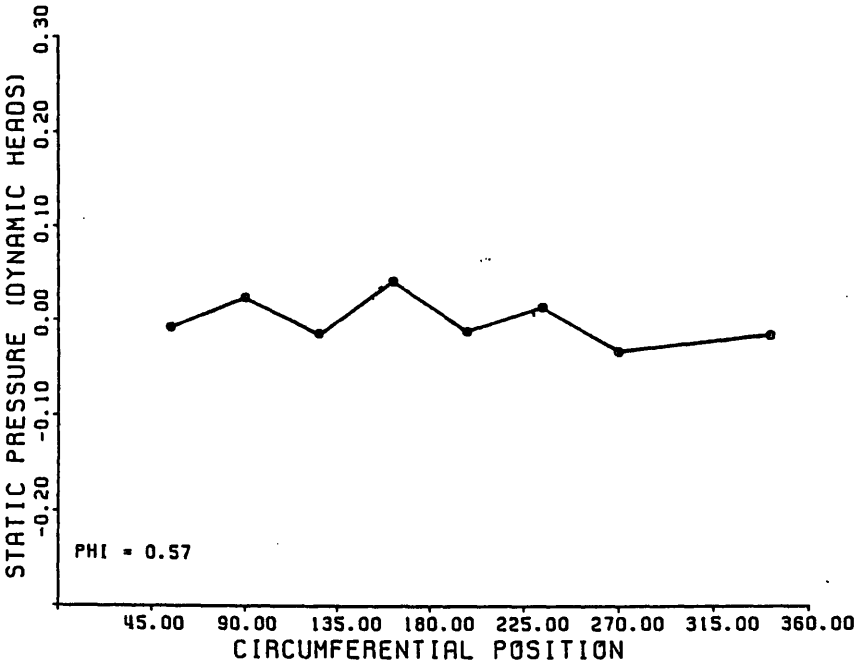

Fig. 4.6 Exit Static Pressure Profile at Design Flow

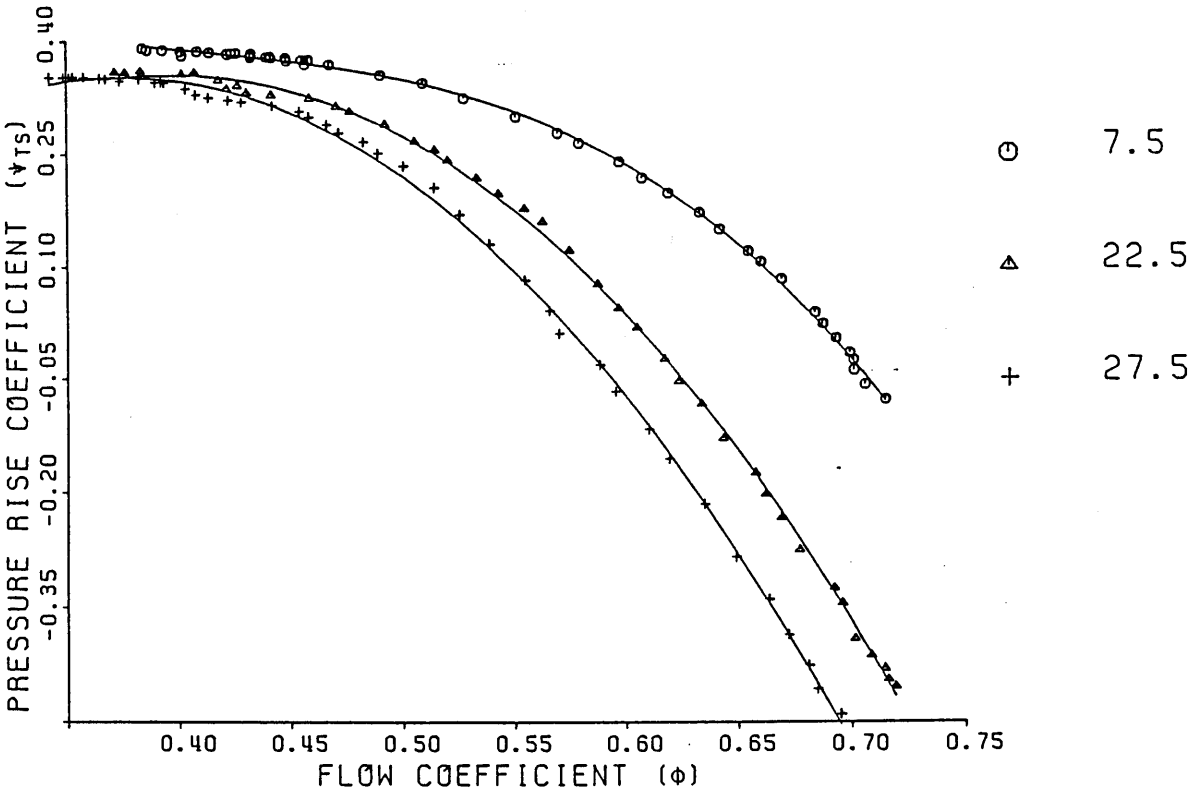

Fig. 4.7 Compressor Speedline Curvefit for Control Variable Calculation

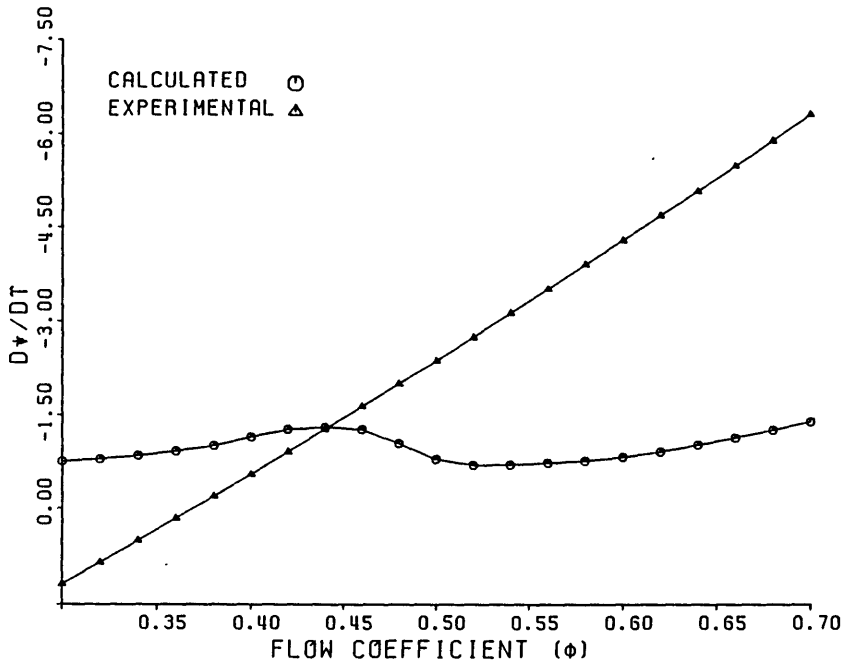

Fig. 4.8 Change in Pressure Rise due to Change in IGV Stagger Angle vs Flow Coefficient

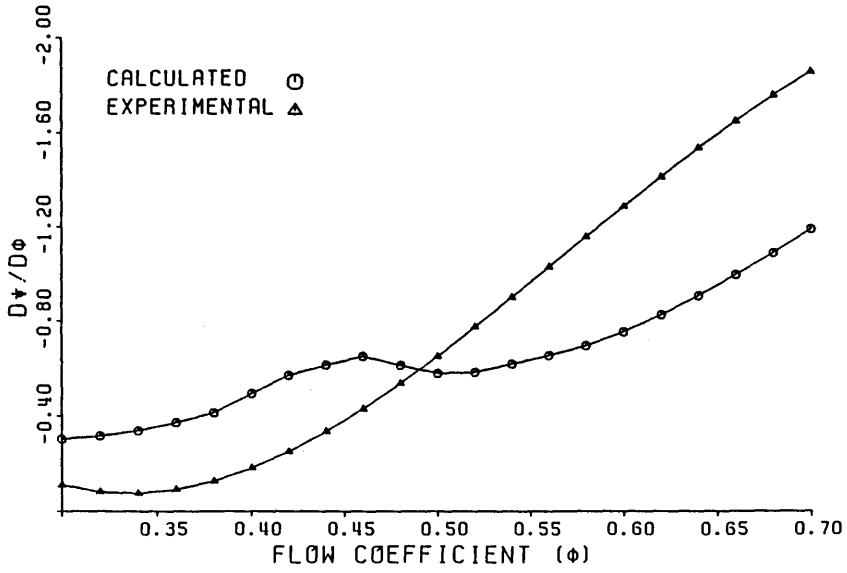

Fig. 4.9 Compressor Characteristic Slope vs Flow Coefficient

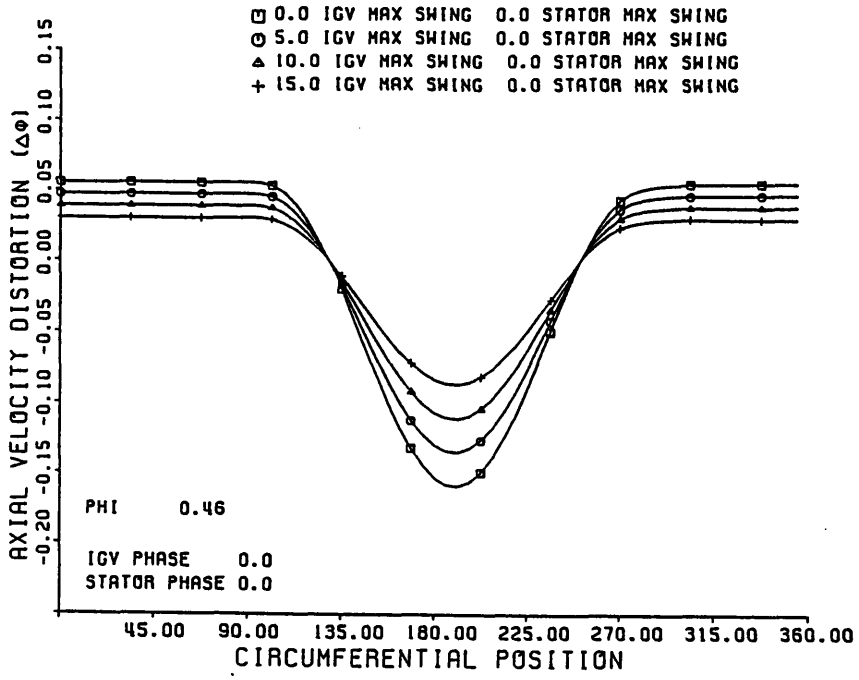

Fig. 4.10 Calculated Compressor Response to a 1.0 Dynamic Head Distortion with 0,5,10,15 Degree IGV Restagger Near Stall

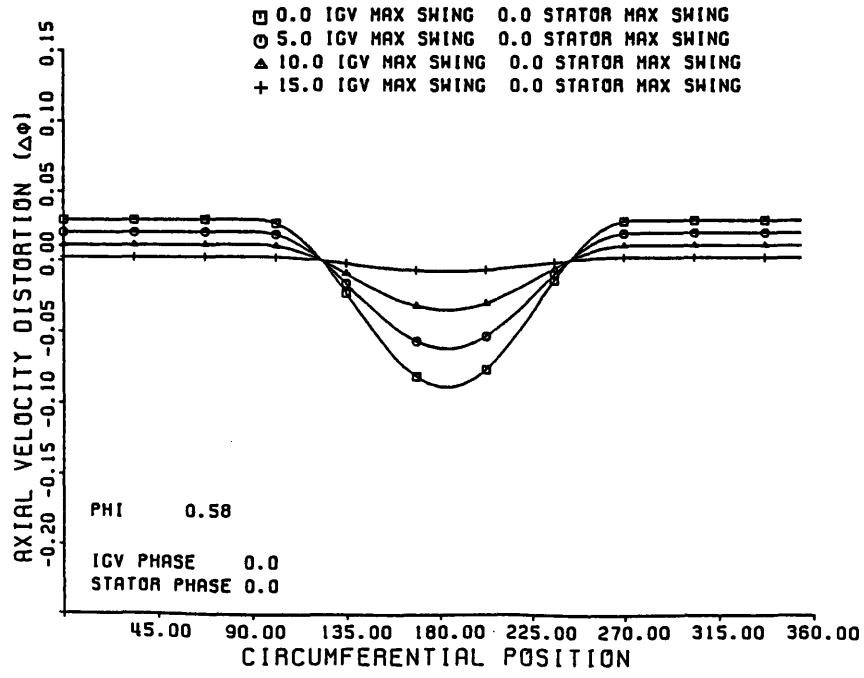

Fig. 4.11 Calculated Compressor Response to a 1.0 Dynamic Head Distortion with 0,5,10,15 Degree IGV Restagger at High Flow Coefficient

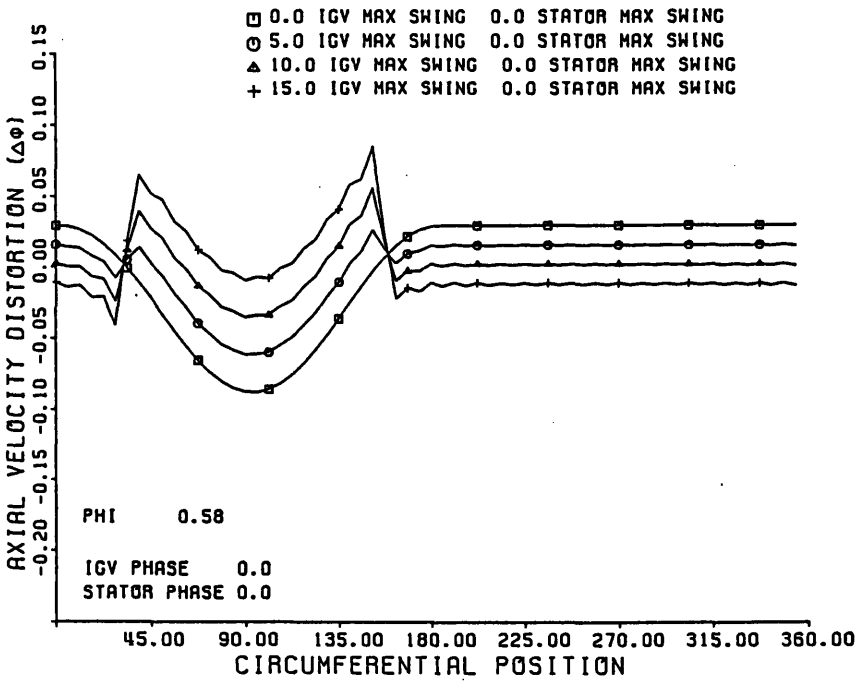

Fig. 4.12 Calculated Compressor Response to a 1.0 Dynamic Head Distortion with 0,5,10,15 Degree Square Wave IGV Restagger at Design Flow

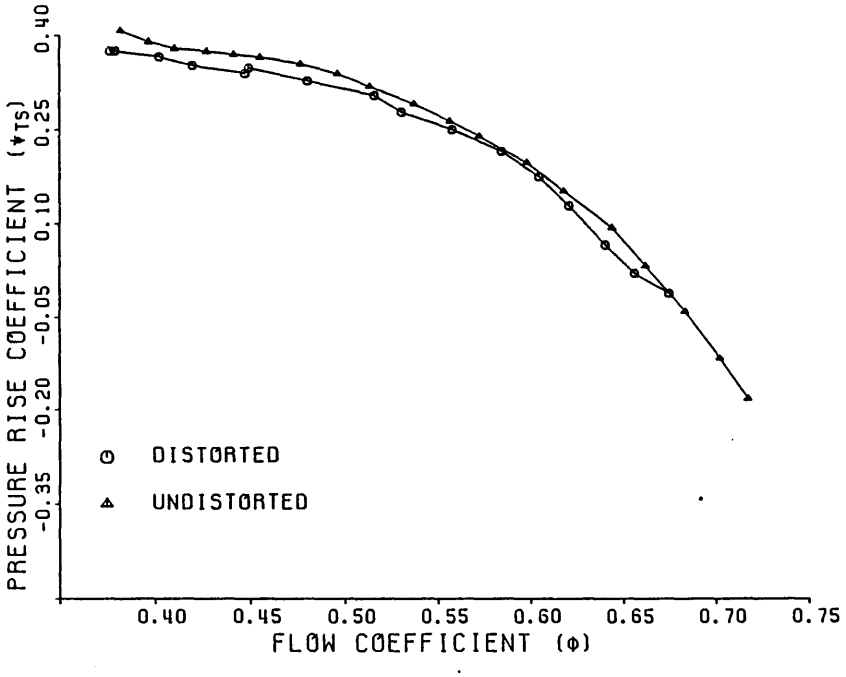

Fig. 4.13 Compressor Speedlines for 15 Degree IGV Stagger with and without Inlet Total Pressure Distortion

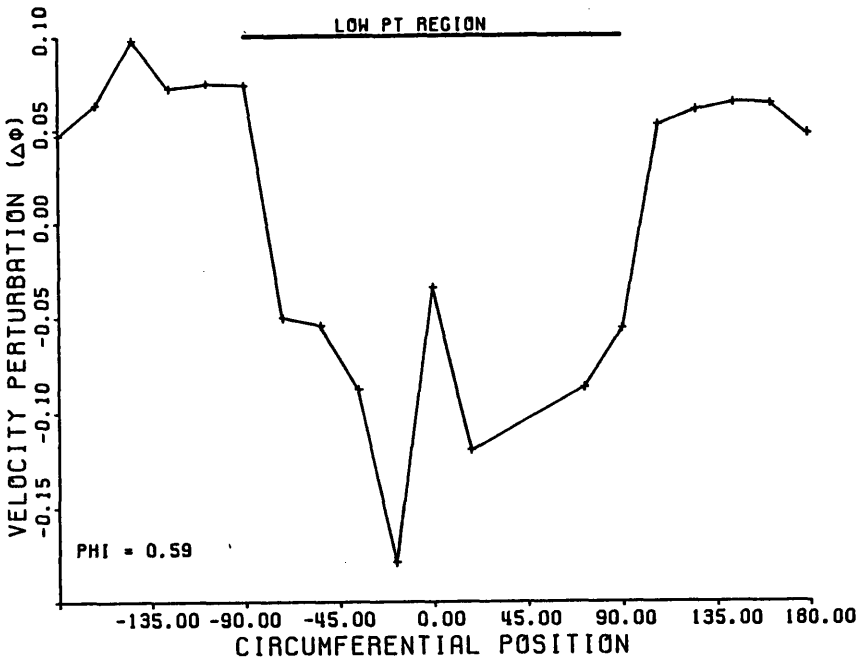

Fig. 4.14 Inlet Velocity Profile for Baseline Compressor with Inlet Total Pressure Distortion Near Stall

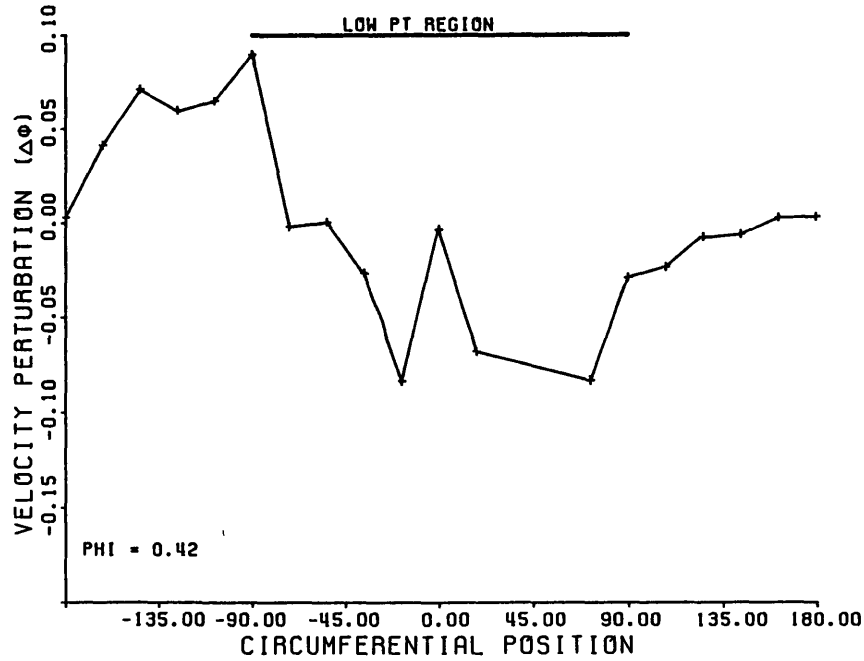

Fig. 4.15 Inlet Velocity Profile for Baseline Compressor with Inlet Total Pressure Distortion at Design Flow

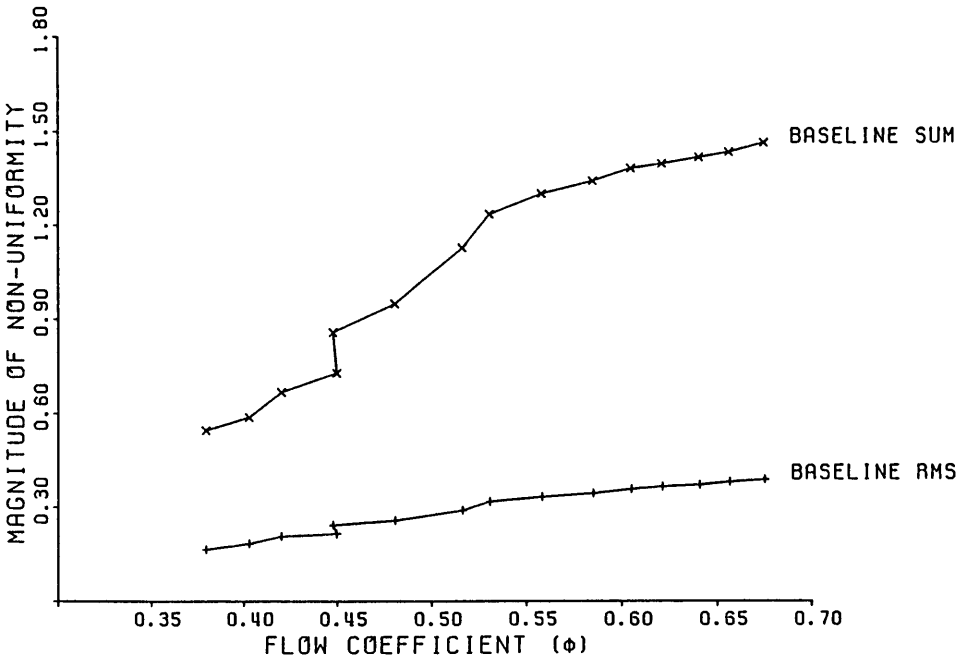

Fig. 4.16 Velocity Non-Uniformities for Baseline Compressor with 1.0 Dynamic Head Inlet Total Pressure Distortion

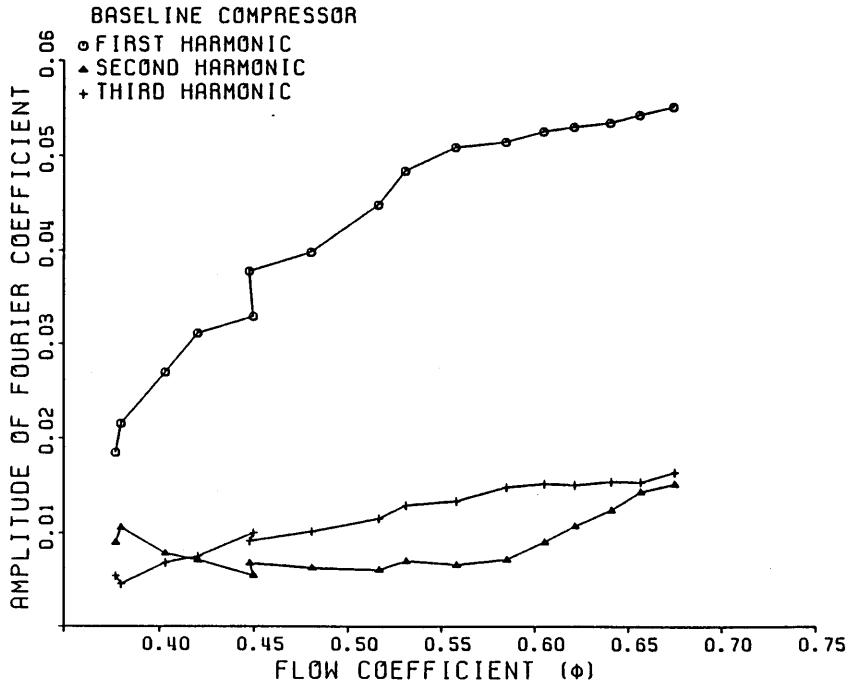

Fig. 4.17 Magnitude of First, Second and Third Fourier Coefficients of Velocity Non-Uniformity for Baseline Compressor with Inlet Total Pressure Distortion

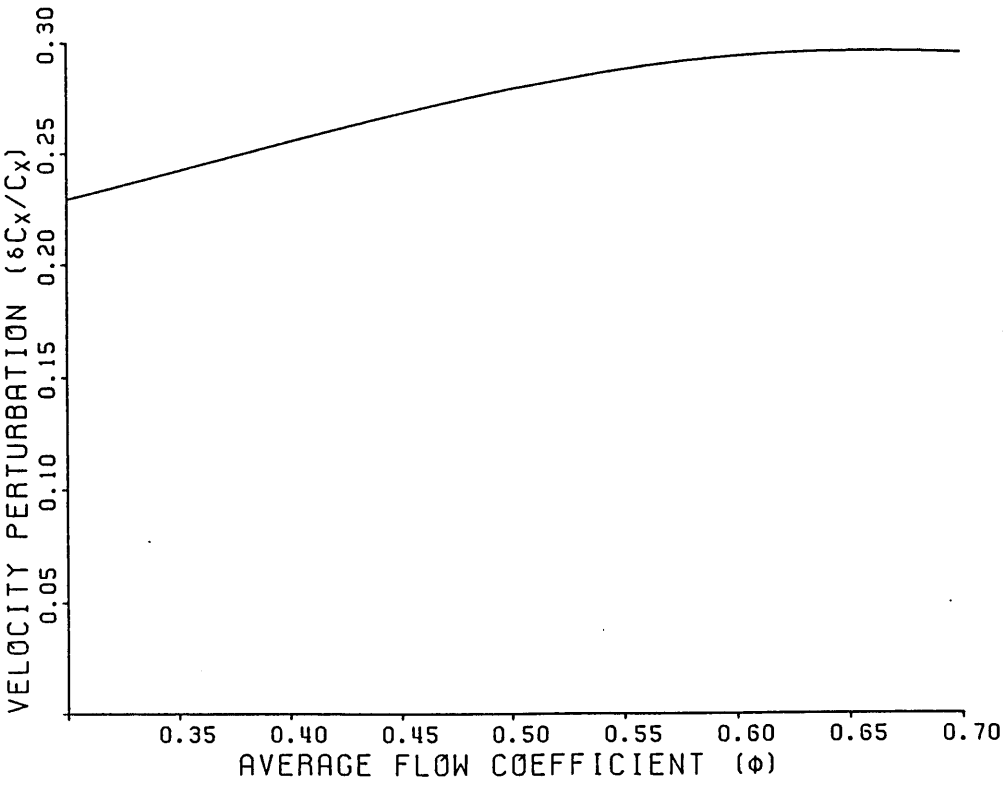

Fig. 4.18 Calculated Magnitude of Axial Velocity Perturbation for a Isolated Rotor with a 10% Inlet Velocity Non-Uniformity

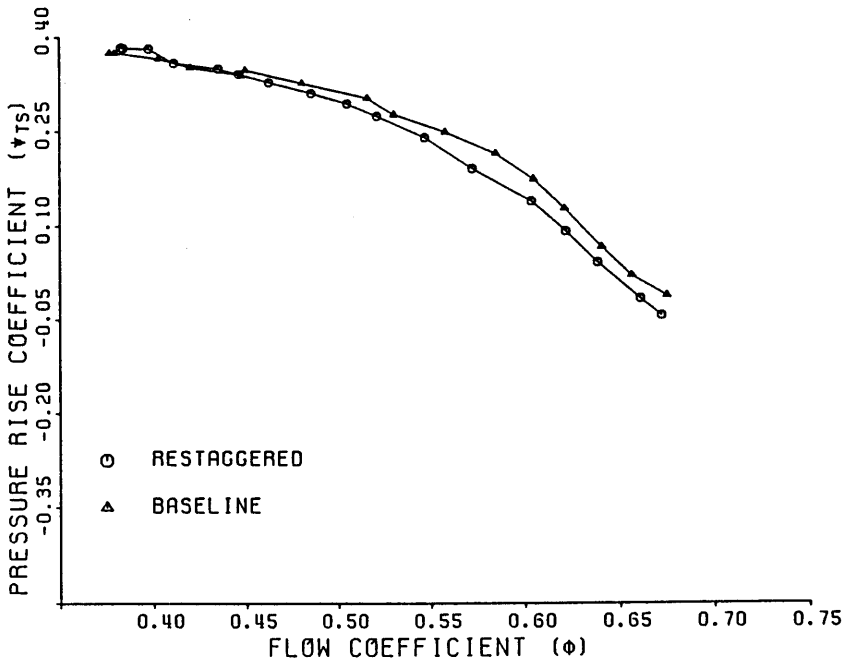

Fig. 4.19 Restaggered and Baseline Compressor Speedlines with Inlet Total Pressure Distortion

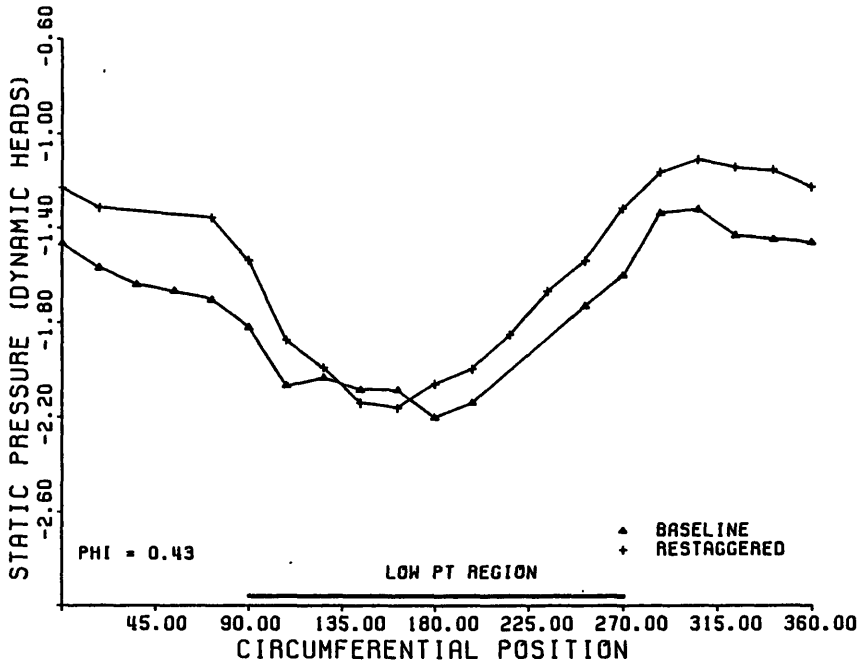

Fig. 4.20 Inlet Static Pressure Profile for Baseline and Restaggered Compressor Near Stall

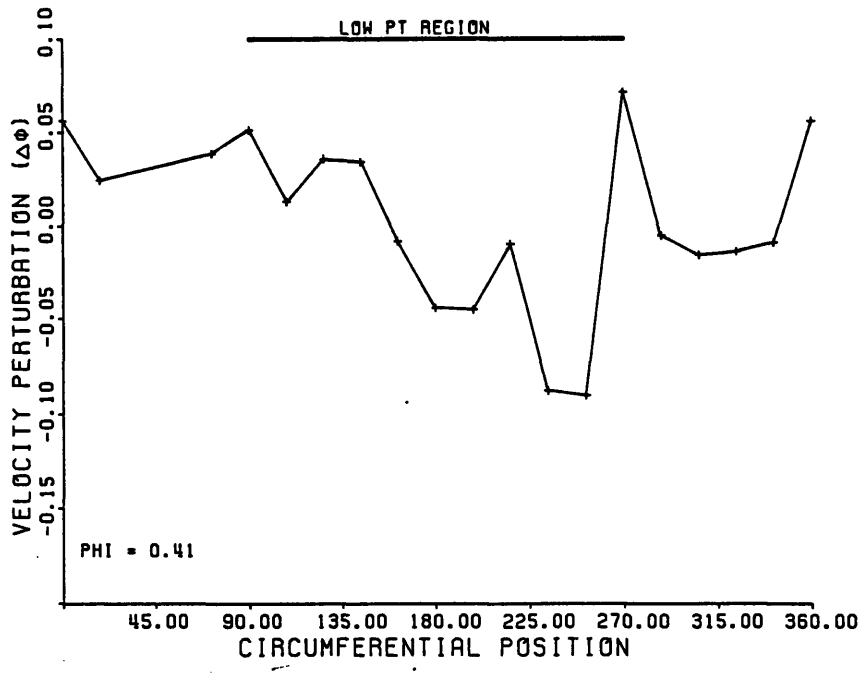

Fig. 4.21 Inlet Velocity Profile for Compressor with Total Pressure Inlet Distortion and IGV Restagger Near Stall

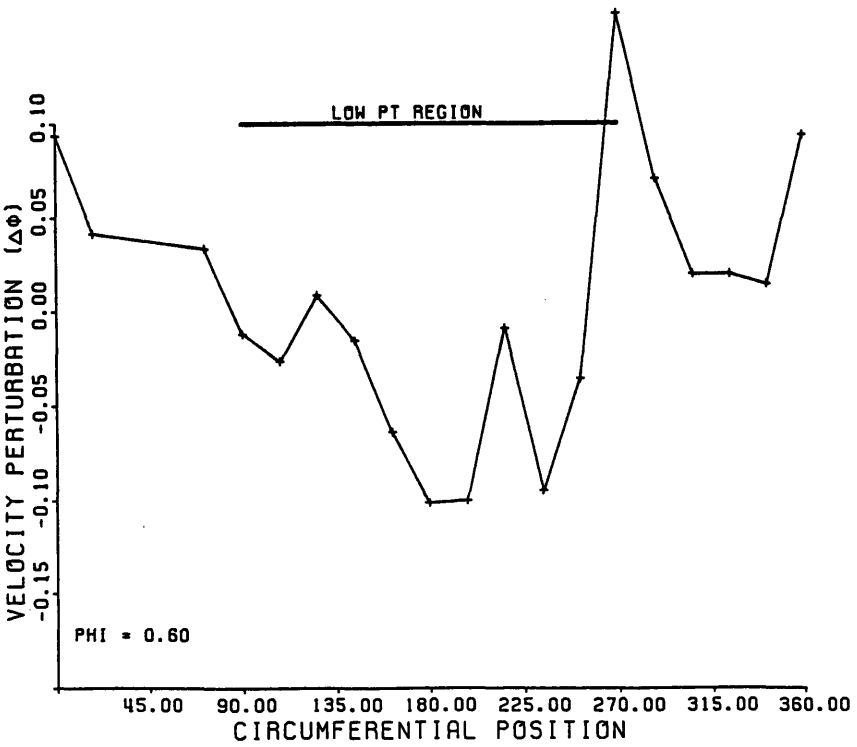

Fig. 4.22 Inlet Velocity Profile for Compressor with Inlet Total Pressure Distortion and IGV Restagger at Design Flow

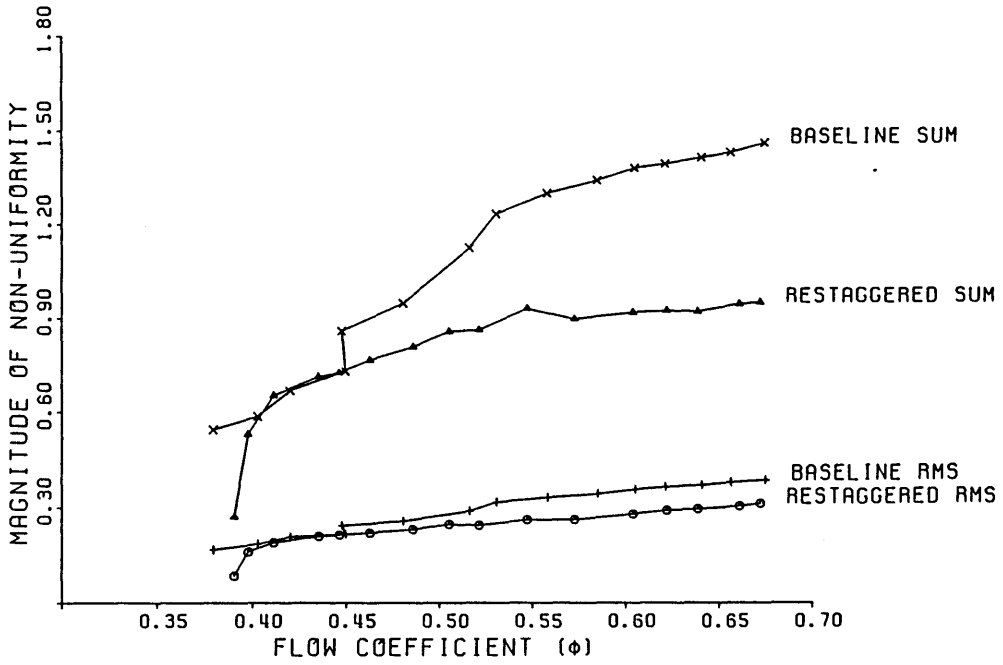

Fig. 4.23 Velocity Non-Uniformities for Baseline and Restaggered Compressor with 1.0 Dynamic Head Inlet Total Pressure Distortion

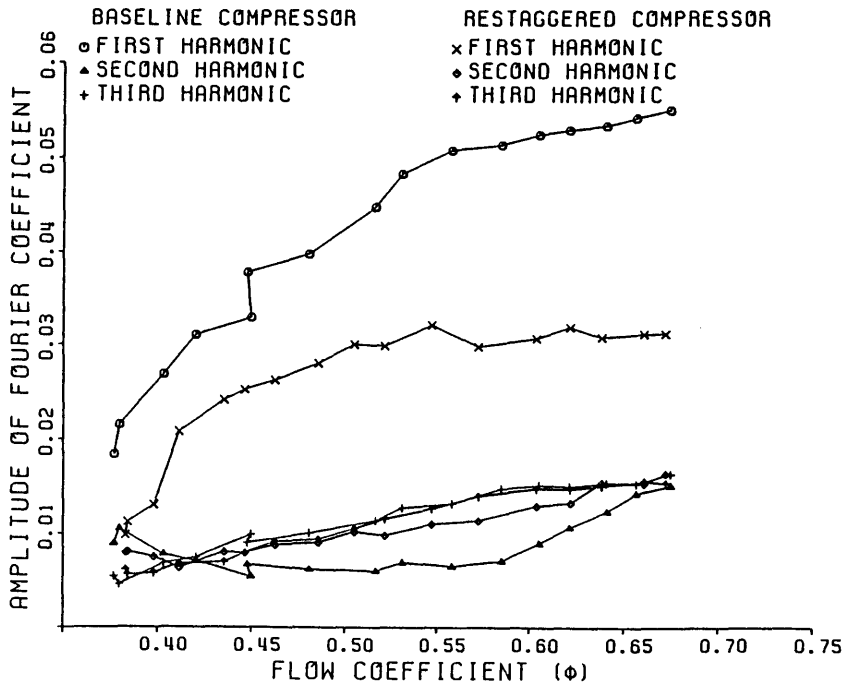

Fig. 4.24 Magnitude of First, Second and Third Fourier Coefficients of Velocity Non-Uniformity for Baseline and Restaggered Compressor with Inlet Total Pressure Distortion

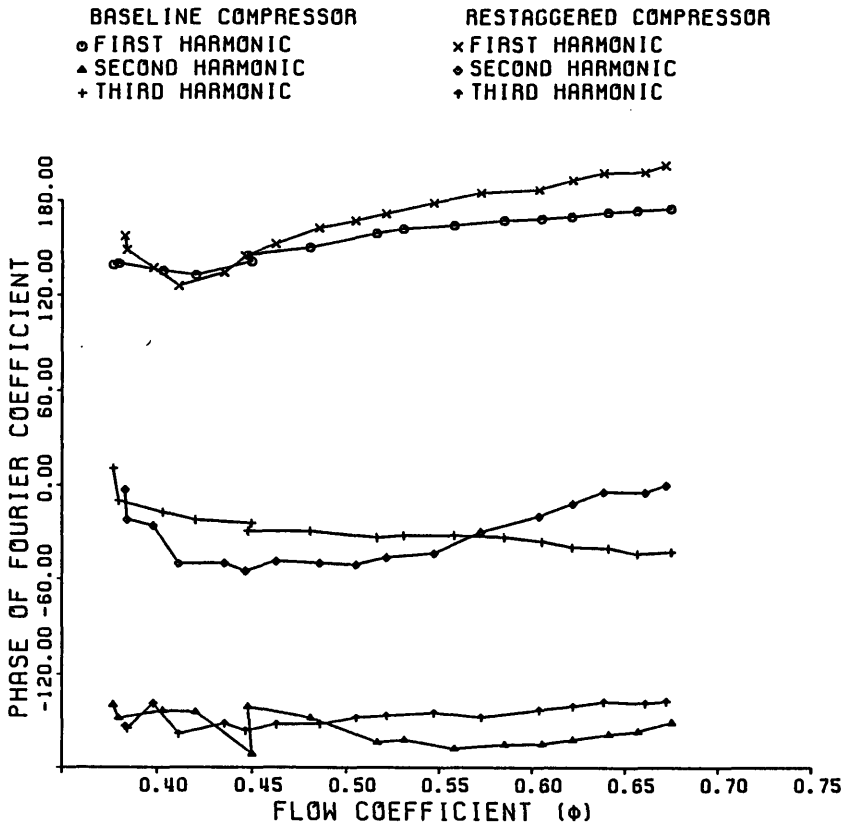

Fig. 4.25 Phase of First, Second and Third Fourier Coefficient of Velocity Non-Uniformity for Baseline and Restaggered Compressor with Inlet Total Pressure Distortion

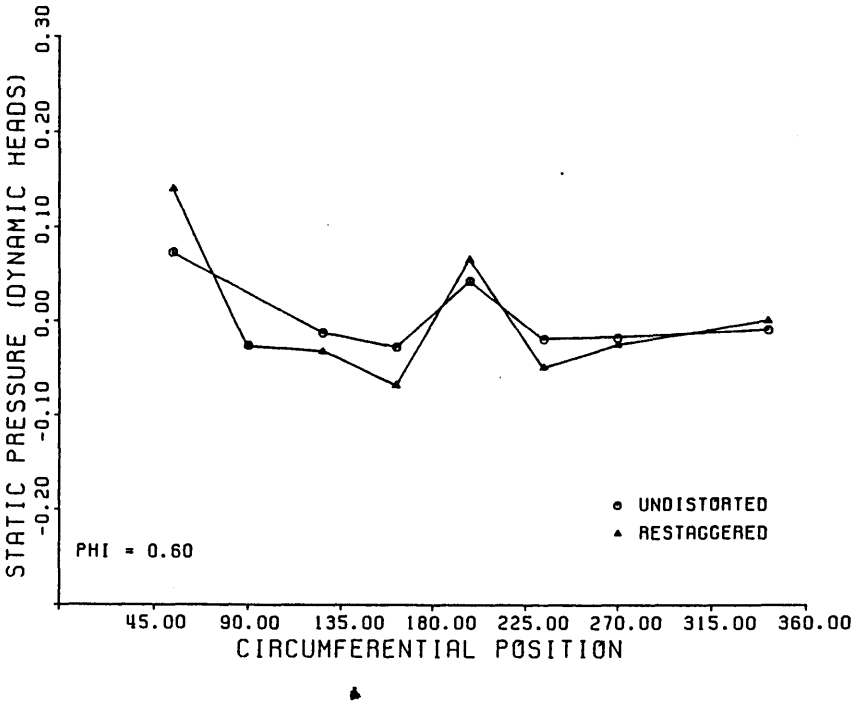

Fig. 4.26 Exit Static Pressure Profile for Undistorted and Restaggered Compressor with Inlet Total Pressure Distortion at Design Flow